DOE/ET/12099-1

THE OXIDATION/GASIFICATION OF RETORTED OIL SHALE

Final Report (Anvil Pts Shale)

By
William J. Thomson

October 1979

Work Performed Under Contract No. AS07-77ET12099

Department of Chemical Engineering
University of Idaho
Moscow, Idaho

U. S. DEPARTMENT OF ENERGY

DISCLAIMER

DISCLAIMER

Available from the National Technical Information Service, U. S. Department of Commerce, Springfield, Virginia 22161.

Price: Paper Copy $8.00
Microfiche $3.50

DOE/ET/12099-1
Distribution Category UC-91

THE OXIDATION/GASIFICATION OF RETORTED OIL SHALE

FINAL REPORT (ANVIL PTS SHALE)

William J. Thomson

Department of Chemical Engineering
University of Idaho
Moscow, Idaho 83843

October 1979

prepared for

U.S. Department of Energy
under Contract No.
DE-AS07-77ET12099

University of Idaho

College of Engineering

SUMMARY

Reaction rate kinetics have been determined for the oxidation and gasification of oil shale char produced by retorting oil shale from the Anvil Points area of Colorado. Experimental methods employed included continuous gravimetric measurements as well as chromatographic analyses of the make-gas. Variables which were investigated included the effect of retorting rate (.3-17 °C/min) on the char quantity and quality as well as a range of concentrations and temperatures pertinent to char gasification. Specifically these included temperatures from 425 C to 800 C, oxygen partial pressures from .03 to .21 atm, CO_2 partial pressures from .01 to 1.0 atm and steam partial pressures from 0.18 to 0.75 atm. In addition a number of experiments were conducted to determine oxygen mass transport limitations for larger (2 cm diameter) cylindrical core samples.

It was found that as long as the shale was retorted at rates higher than 0.3°C min or with purge velocities higher than 4 cm/min (STP), there was no effect of retorting on the char make. Neither did the assay of the shale (15-50 GPT) have any effect on the char oxidation activity. The kinetic study indicated that char oxidation was first order with respect to both char and oxygen and had an activation energy of 23.2 kcal/mole. These results were valid for shale which were either acid leached or had not undergone mineral decomposition. On the other hand, the CaO produced by the decomposition of calcite appeared to catalyze char oxidation so that its rate was increased by about one order of magnitude. Oxygen mass transfer measurements with the larger shale pieces yielded effective ash layer diffusivities in agreement with previous work and pointed to the importance of convective mass transport during the oxidation of the first 40% of the char.

Limited studies of the mineral reactions which take place indicated that calcite was easily reformed from CaO, particularly when CO_2 was

liberated at the surface from char oxidation. Whereas a reversible calcite decomposition rate expression derived here differed from one produced at Lawrence Livermore Laboratories (LLL), it was found that LLL's silication rate expression provided a good match to the experimental data. The data obtained here regarding the effect of H_2O on mineral decomposition are in agreement with LLL's results although they tend to underestimate the effect. Analysis of the decomposition data during dolomite decomposition point to the possibility that CO_2 may inhibit the decomposition rate as well as prevent steam enhancement.

A rate expression was derived to describe CO_2-char gasification and accounts for low apparent CO_2 reaction orders at high partial pressures. It was also found that it was necessary to consider the role of the water gas shift reaction during steam gasification of the char. Failure to do so results in the prediction of char consumption rates which are significantly higher than measured when conducted in the presence of CO_2-H_2O mixtures. There is also strong evidence to support the contention that iron present in the shale catalyzes steam gasification, particularly the water gas shift reaction. The steam gasification rate was found to be half-order with respect to steam, first order with respect to char, and had an activation energy of 20.6 kcal/mole.

TABLE OF CONTENTS

INTRODUCTION

Even though the current economic scene appears tenuous to prospective investors, particularly when it comes to the development of an oil shale industry in the United States, it is probably only a matter of time before our vast oil shale deposits are utilized. Towards this end it is extremely important that a vigorous research and development program be maintained so that oil shale technology is on a firm fundamental basis when utilization becomes economically feasible.

An overwhelming consideration in the development of an oil shale industry is proper respect for possible environmental damage. The most advanced technology being considered for recovering oil from oil shale involve surface retorting processes. Whereas air and water pollution problems associated with these processes are similar to other related industries, one specific problem is particularly distressing to environmentalists, the problem of ash disposal. Various considerations will probably dictate that the ash emanating from an above-ground process be piled up and revegetated. The characteristics of this ash are important for both practical and aesthetic reasons. When the kerogen compounds contained in raw oil shale decompose to form a type of crude oil, they generally leave behind a carbonaceous residue, or "char." If surface processing stops here, the ash leaving the plant will contain this char and have a deep black color.

Environmental consideration is only one reason for attempting to remove the char. Another reason is to take advantage of its heating value. As Dockter[1] has shown, for oil shales assessed at greater than 20 gallons per ton (GPT), there is more than enough energy in the char to supply the additional heat required for retorting the raw shale. Clearly there would be a needless and expensive waste of energy if the char were not utilized. As might be expected, there are various technical problems associated with the recovery of this energy. For one, attempts to oxidize (burn) it in air can lead to locally high temperatures (~1100C) with resultant problems

of clinker formation and loss of permeability. Another detrimental feature of these high temperatures is the mineral reactions which take place. Depending on the gaseous environment and the temperature time history seen by the shale, a number of decomposition and solid-solid reactions will occur. At least one of these products, CaO, can pose environmental problems since its combination with run-off water could result in high pH soils. In addition, several of the decomposition reactions are highly endothermic, which reduces the thermal efficiency of the process.

Another way in which to utilize the char on retorted oil shale is to gasify it. This would involve reactions of oxygen, CO_2, and steam with the char; the former in order to produce sufficiently high temperatures for the latter to take place. The objective of gasification would be to produce a low-to-medium BTU gas which could be burned elsewhere in the process. Here the kinetics can be quite complex since a variety of reactions can occur some of which can be catalyzed by the alkali components also present in the retorted shale. For surface retorting, the decision whether or not to gasify the char is tied very closely to economic considerations. Such factors as the quantity of steam which must be supplied, the composition of the product gas and the required temperatures must all be carefully evaluated so that decisions can be made on the need for an oxygen plant and the extent of gas treating which will be required. To date only Union Oil Company of California has announced a surface retorting process which would utilize steam gasification, the so-called Steam Gas Recirculation (SGR) process[2]. Here too, a knowledge of the reaction kinetics would contribute to the development of oil-shale technology.

A knowledge of the kinetics of the oxidation/gasification of the char on retorted oil shale is not only desirable for improving the technology of surface retorting, but is even more important for *in-situ* oil shale retorting. This process has some very attractive environmental and economic features since it avoids the problems of ash disposal and solids handling.

Most development work has centered on modified in-situ processes which involves some mining in order to be able to create a "chimney" of broken shale. In this case there is always direct utilization of the char since it fuels a combustion front which gradually moves down the chimney. The gases moving through the front are heated and move downstream where they give up their heat to the cooler shale which gradually reach retorting temperatures (~450C). The char left behind then serves as the fuel to the combustion front when it eventually reaches the retorted shale.

The cost of compressing the large quantities of air necessary to form the combustion zone can be extremely high and the process generally produces a low quality off-gas which must be flared or burned. There would be a tremendous advantage if a higher quality gas could be produced so that it would contain sufficient energy to supply the needs of the entire process. Preliminary work at Laramie Energy Technology Center (LETC)[3, 4] has shown that a combination of oxidation and gasification can indeed produce such a gas. There are currently two in-situ development programs which are using steam in the sweep gas; the Rio Blanco Project[5] and Equity Oil's BX Project[6]. In the latter case, the inlet sweep gas is 100% steam.

A knowledge of the kinetics of the various char reactions which can take place is not only important for surface retorting process design but also as inputs to the various predictive mathematical models which attempt to describe in-situ retorting. In this latter case accurate models can be used to update the progress of the retorting and to hopefully lead to corrective controls if and when problems arise with maldistribution, loss of permeability, and the like.

The work which has been conducted to date in the Department of Chemical Engineering at the University of Idaho has dealt only with Colorado oil shale, specifically with shale from the Anvil Points area of Colorado. This report describes the results of separate sets of experiments to

determine kinetic expressions for the oxidation, CO_2 gasification, and steam gasification of oil shale char. These were all studied under conditions where only reaction kinetics should predominate and for a wide range of reactant concentrations and temperatures. In addition, the reactivity of the char for different assay shales and for a range of retorting conditions was also determined. Because of the fact that a number of these reactions will occur simultaneously in an actual retort, one series of experiments was designed to study kinetic interactions with two or more reactive components. Finally, because of the high rates of char oxidation, global oxidation rates were determined for larger shale pieces in order to quantify the role of gas-solid and ash diffusion mass transport.

This project was supported by the Department of Energy under contract number DE-AS07-77ER12099 and was under the technical direction of Leroy Dockter at the Laramie Energy Technology Center (LETC).

BACKGROUND

Although oil shale processing, particularly surface retorting, has been in development for about 30 years, very little work dealing with rate processes was accomplished prior to 1970. However, with the renewed interest in the development of a synthetic fuels industry in this country, this situation has changed markedly over the past 5 years. In order to be as brief and pertinent as possible, this section of the report will only deal with previous kinetic and rate studies which have a direct bearing on the work reported here. What is more, this discussion is subdivided into the various oil shale reactions which can take place; i.e., pyrolysis, mineral reactions, and the oxidation and gasification of char.

Pyrolysis

Because there are indications that the retorting rates may affect the activity and the quantity of char left behind on the shale, it is appropriate to mention some of the previous studies which have been conducted on kerogen decomposition rates; i.e., oil shale pyrolysis. The first extensive study of kerogen decomposition rates was conducted by Hubbard and Robinson in 1950[7]. They reported that the decomposition rates were first order with respect to the organic matter present and were a function of temperature. They presented an Arrhenius type expression for the specific rate constant as a function of temperature. These original data were reanalyzed by Allred[8] in light of his own thermogravimetric data. He concluded that the reaction mechanism was a set of series reactions by which the kerogen first decomposed to gas, bitumen and char and the bitumen subsequently decomposed to hydrocarbons. Whereas Hubbard and Robinson conducted their experiments isothermally and Allred heated his shale samples very slowly (3°F/min.), Arnold[9] has reported on his study of kerogen decomposition rates utilizing various heating rates. He concluded that higher heating rates produced higher decomposition rates, resulted in higher boiling components in the recovered shale oil and increased the quantity of char. Although kinetic interpretations of these data are difficult, there seems to be little question that the heating rates

definitely affect the character of the char. A more recent study at Lawrence Livermore Laboratories[10] showed that additional coke-like-char could be produced during pyrolysis if the kerogen decomposition products were not rapidly removed from the shale. This was attributed to the cracking of products and was found to increase at low carrier gas flow rates and low heating rates during retorting.

Mineral Reactions

In addition to kerogen, oil shale contains a mixture of a variety of mineral carbonates and silicates as well as various quantities of iron, aluminum and sodium. Anvil Points shale contains significant amounts of dolomite and calcite, both of which decompose in inert environments at about the same temperatures. The presence of a large amount of silica also allows the mineral carbonates to decompose to both silicates and oxides. The presence of a small amount of minerals known to be catalysts for many reactions, are also found in the shale. Studies conducted on the mineralogy[11-13] have shown that the mineral composition of the oil shale is very sensitive to the temperature and to the external gas composition to which the shale has been exposed. Similarly the surface characteristics may also vary during a reaction and thus alter the ability of the shale to undergo certain reactions. The size, geometry, and initial conditions of an oil shale sample can have a very dramatic effect on the gas environment at the reacting surfaces of the shale. It is therefore very important that the manner in which the experiments were performed in the earlier studies be noted as a means to explain any discrepancies in the results of these studies and to gain insight into the true kinetics of the reactions being considered.

Both dolomite and calcite are known to decompose in an inert atmosphere at elevated temperatures to MgO and CaO. Whereas dolomite can decompose to calcite in a CO_2 rich environment, calcite decomposition is reversible and can be inhibited by the presence of CO_2. Actually, dolomite decomposition may proceed by two reaction paths during decomposition:

$$CaMg(CO_3)_2 \rightarrow MgO + CaO + 2CO_2 \quad (PCO_2=0) \qquad (1)$$

$$CaMg(CO_3)_2 \rightleftarrows MgO + CaCO_3 + CO_2 \quad (PCO_2\neq 0) \qquad (2)$$

Calcite decomposition follows only one reaction path during decarbonation:

$$CaCO_3 \rightleftarrows CaO + CO_2 \qquad (3)$$

The reversible nature of this reaction is very sensitive to relatively low partial pressures of CO_2.

Mineral analyses of raw Anvil Points oil shale reveal that a small portion of the dolomite in the shale is in fact Ankerite ($CaFe(CO_3)_2$) in which the magnesium in the dolomite has been replaced by iron. The decomposition of ankerite is generally considered to follow the same reactions as the dolomite except that Fe_2O_3 and Fe_3O_4 are the ultimate products containing iron instead of FeO[13]. Because there is an abundance of quartz present in the shale it has been found that the dolomite and calcite can also react with the quartz to produce a large number of calcium and magnesium silicates. All of the reactions involving quartz have been found to be irreversible, resulting in the evolution of CO_2 according to the generalized expression:

$$MCO_3 + \text{silica} \rightarrow \text{silicate} + CO_2 \qquad (4)$$

where "M" represents the minerals Ca and Mg. The principle silicates formed are ankermanite ($Ca_2MgSi_2O_7$) and diopside ($CaMgSi_2O_6$).

One of the earliest kinetic studies of mineral decomposition in oil shale was performed by E. E. Jukkola, et. al.[14]. He studied the isothermal decarbonation of raw 30 GPT Green River oil shale ground to 65 mesh. In his experiments, 10 gram samples were placed in a one inch diameter sample holder, which were then placed in a reactor preheated to a desired temperature. The samples were reacted at this temperature for a specified length of time and then removed from the reactor and quenched. In each experiment either pure CO_2 or nitrogen was percolated through the sample holder and at the end of the run, the mineral CO_2 remaining in the sample was determined. The experiments were performed over a range of temperatures from 565 C to 870 C.

The kinetics for dolomite decomposition were determined by taking the rate of CO_2 evolution for the first 25% of the total CO_2 evolved and assuming during this period that the calcite was not decomposing. A first order reaction analysis for dolomite gave a rate constant with an activation energy of 48 kcal/mole for decomposition in one atmosphere of CO_2 and 98.4 kcal/mole for decomposition in nitrogen. It was found that the decomposition rate of

dolomite in the CO_2 atmosphere was as much as 6 times faster than that in the nitrogen mixture but no explanation was given. Their analysis of the decomposition of calcite was accomplished by measuring the rate of CO_2 evolution for the final 68% of the total CO_2 evolved and making the assumption that only calcite was decomposing during this portion of the run. An activation energy of 89.2 kcal/mole was calculated for calcite decomposition assuming first order kinetics for both gas environments. No mention of the effect of reversibility on the accuracy of the rate expression was discussed.

Won C. Park, et. al.[13] performed a series of experiments using oil shale from the Logan Wash site in Colorado. His experiments were similar in many respects to those of Jukkola, at. al.[14]. All experiments were performed by introducing an unretorted 8.4 GPT oil shale sample into a reactor which had been preheated to a desired temperature. The sample was removed after a specified time and cooled. The experiments covered a temperature range from 600°C to 1200°C and used sweep gases of either pure CO_2, a 1% O_2/N_2 mixture or air flowing at 5000 cc/min. The mineral composition of the cooled samples was determined principally by x-ray diffraction methods. The dolomite and calcite contents were also measured by reaction with orthoscopic acid after pretreatment. The main difference between the experiments in these two investigations was in the sample preparation. Park used reconstructed oil shale pellets prepared from a homogeneous mixture of Logan Wash shale obtained from a 100 foot deep-shale composite. The composite was ground to a 503 μm diameter powder, mixed, and then pressed at 21,000 psig into one inch diameter pellets. Park's study showed that the decomposition rates for dolomite were first order in dolomite and that MgO and calcite were stable products in the presence of a CO_2 atmosphere at lower temperatures. At temperatures above 800°C the MgO underwent a rapid silication and the calcite reacted with both the quartz and MgO to form various silicates. The major product minerals observed were diopside ($CaMgSi_2O_6$) and akermanite ($Ca_2MgSi_2O_7$). Calcium oxide was not observed as a product in any of the experiments performed. In one set of experiments, performed using a steam-air gas mixture, Park found both the rate of mineral decarbonation and silicate formation to be accelerated due to the presence of steam.

Cambell[15,16] also performed experiments on retorted and decharred oil shale from the Anvil points area. In his experiments, 10-50 mg samples of raw shale were ground to 800 μm and retorted to 500 C at a heating rate of 12°C/min. Oxidation was then conducted in air for 24 hours at 400 C (a temperature below that necessary for decomposition of dolomite and shale). After oxidation, the samples were heated from 500 C to 1000 C in various CO_2-N_2 gas mixtures and at various linear heating rates with a constant sweep gas flow rate of 80 cc/min. The resulting weight loss rate was analyzed for each experiment using a non-linear least squares method to determine the kinetic parameters which fit the reversible decomposition rate expression:

$$d(MCO_3)/dt = (MCO3)(k_f)(1 - PCO_2/Keq) \quad (5)$$

in which MCO_3 represented either dolomite or calcite and k_f was assumed to be the same for both dolomite and calcite decarbonation

$$k_f = 1.0(10)^{12} \exp(-57.8/RT) \quad (6)$$

The equilibrium constant for dolomite decomposition was determined to be large enough to neglect the term P_{CO_2}/Keq in the above expression. The equilibrium constant for calcite decomposition was calculated from other experiments and found to be:

$$Keq = 1.92\ (10)^8\ \exp(-44.4/RT) \quad (7)$$

Campbell also performed experiments on pure nahcolite ($NaHCO_3$) and dawsonite ($NaAL(OH)_2CO_3$); two carbonates which are found in small but measurable amounts in Anvil Points shale. It was concluded from their experiments that these minerals are completely decarbonated at temperatures above 420 C[15].

In Campbell's study of carbonate decomposition, analysis of the thermogravimetric measurements showed a third reaction taking place when the samples were decomposed in a gas environment containing CO_2. This reaction was considered to be due to reactions of the calcite with quartz to produce various silicates. In order to predict the rate of calcite decomposition to the silicates, an empirical rate expression was formulated which

assumed an activation of 27.2 kcal/mole as reported by Kridelbaugh[17] for the reaction between pure calcite and silica. The rate expression also assumed that the weight loss observed was due only to reactions between the quartz and calcite to form calcium silicate. The formation of magnesium silicates was assumed to come about from reactions between the MgO and the silicates rather than directly from the decomposition of dolomite. The final model involved two expressions to characterize the reaction of free calcite with silica and the reaction of calcite produced from dolomite decomposition, with silica. The rate expressions are respectively:

$$d(CaCO_3)_f/dt = 2.5(10)^5 \exp(-27.2/RT)(CaCO)_f(a_{CaO}) \quad (8)$$

$$d(CaCO_3)_d/dt = 1.5(10)^4 \exp(-27.2/RT)(CaCO_3)_d(a_{CaO}) \quad (9)$$

Where:

$$a_{CaO} = Keq/P_{CO_2} \text{ for } P_{CO_2} \geq Keq \quad (10)$$

$$a_{CaO} = 1.0 \text{ for } P_{CO_2} < Keq \quad (11)$$

Campbell acknowledged that the above rate expressions are, at best, simple empirical models based on observation rather than solid state reaction mechanisms.

Burnham[11,16] performed mineral decomposition experiments in the presence of steam. Using shale samples from the same master batch used by Campbell[15], they were also retorted and decharred in the same manner. The sample size used in these experiments was typically .25 g and a sweep gas flow rate of 1500 cc/min was used. Reaction rates were determined by measuring the CO_2 evolution rates during a linear heat up rate of 2.1 C/min from 400 C to 900 C. In a second set of experiments, samples weighing about 0.8 g were added to a reactor which had been preheated to 400 C. The samples were then heated at 4 C/min to a specified temperature and then removed from the reactor. The samples were immediately cooled and analyzed for mineral content using x-ray diffraction analysis. A purely empirical kinetic model was developed which describes the rate of dolomite

and calcite decomposition in the presence of steam. The general expression is:

$$d(MCO_3)/dt = [f_1 R_1 + f_2 R_2](MCO_3) \quad (12)$$

Where: $f_1 = .35\ P_{H_2O}$ (13)

$f_2 = 1 - f_1$ (14)

$R_1 = 60(\exp[23.9 - 5.45\ P_{H_2O}])(\exp[52.0 - 12.6\ P_{H_2O}]/RT)$ (15)

$R_2 = 60\mathrm{Exp}(23.9 - 5.45\ P_{H_2O})\ \exp(57.0 - 12.6\ P_{H_2O})/RT)$ (16)

This expression, when extrapolated to 0% steam, gives a reaction rate that is twice that predicted by Campbell[15] for the same conditions. No explanation was given for this discrepancy.

A considerable discrepancy exists in the activation energy for dolomite and calcite decomposition, between those predicted by Jukkola et al[14] and those reported by Campbell[15]. Other studies on the decomposition of pure calcite referenced by Campbell give activation energies that range from 40 to 52.5 kcal/mole[18]. These values agree fairly with Campbell's results for shale, and with his activation energy of 55.5 kcal/mole obtained with pure calcite. Jukkola et al[14] referenced the results of Ralston et al[19] along with some of their own results for the decomposition of pure calcite, which give an activation energy of 140.9 kcal/mole. Young[20], in his discussion of the decomposition of pure dolomite and pure calcite, showed that the activation energies ranged from 44 kcal/mole to 55 kcal/mole for dolomite and 40 kcal/mole to 41 kcal/mole for calcite. Burnham's[11] experiments were similar to those run by Campbell, but the kinetics were determined using CO_2 evolution rates. He found the dolomite and calcite decompositions to have an activation energy of 57 kcal/mole. It would seem that the kinetic expressions developed by Campbell are in better agreement with the other works than those of Jukkola et al[14].

Another interesting difference in the results reported by the various authors on the decarbonation of calcite present in oil shale, is on the

production of CaO as a product of decarbonation. Park[13] did not observe CaO as a product of decarbonation in any of his experiments where x-ray diffraction analysis was used. Similarly, Smith et al[21], in his x-ray diffraction studies of mineral products resulting from the decarbonation of mahogany zone (Colorado) oil shale at temperatures ranging from 300 C to 1100 C and in atmospheres of air, nitrogen, and CO_2, found CaO as a product only when the shale was decomposed at 900 C with nitrogen used as the carrier gas. Burnham[11], in his x-ray diffraction analysis of samples decarbonated in various gas mixtures of N_2, steam, and CO_2, showed CaO to be a major product when the shale was decomposed in nitrogen, and a measurable product when 50/50 mixtures of steam and CO_2, nitrogen, and CO_2, and nitrogen and steam were used.

There are two possible explanations for the apparent discrepancies in these results. The first possible cause could be the difference in the sample size. Although details of the sample size and preparation in Smith's studies were not provided, Park used one inch diameter pellets. Burhnam, on the other hand, used powdered samples ranging from 250 to 800 mg. It is very possible that the samples used by Park were large enough that the CO_2 partial pressures inside the pellet were of sufficient magnitude to prevent the decomposition of calcite to CaO (since it is reversible), thus allowing the calcite to decompose entirely to the various silicates. A second possible cause for the difference in the results is due to the difference in the initial condition of the sample. Park used unretorted shale in his experiments which were subsequently retorted at the high temperatures necessary for decomposition of dolomite and calcite. The gas environment experienced inside the pellets during this retorting process would be significantly different than the retorted and decharred samples used in the experiments by Burnham. Although there is no proof, it is possible that the presence of O_2 in the experiments performed by Smith and Park may have inhibited CaO formation in those runs without CO_2 in the sweep gas.

Char Oxidation

The first experimental studies of oil shale char oxidation dealt with relatively large particles since these are expected to be predominant for in-situ retorting.

One of the first studies of this nature was conducted by Dockter[1] who studied the oxidation of cylindrical core samples of shales which assayed at 10-40 gallons per ton (GPT). He found that for oxygen concentrations between 7 and 21% and for temperatures between 400 and 600 C that the burn depth pattern followed a diffusion control shrinking core model. This was followed by a study conducted by Mallon and Braun[22] who experimented with large blocks of oil shale (0.15-0.25 m) and studied the oxidation as well as the reactions of CO_2 with the char. They also found that the oxidation rate was limited by diffusion and concluded that the reaction rate of the CO_2 (released by carbonate decomposition) with the char was significantly higher than the diffusion limited oxidation rate. As can be seen, prior to the work reported here, there was little research effort expended on the subject of char oxidation and essentially no true kinetic data.

CO_2 Gasification

Carbon dioxide can react with the char to produce carbon monoxide according to the reaction:

$$CO_2 + C \rightarrow 2CO \tag{17}$$

In a study of the gasification of pulverized coal[18], a reaction scheme using Langmuir Hinshelwood kinetics was based on the mechanism:

$$CO_2 + S \rightarrow CO + S{\cdot}O \tag{18}$$

$$S{\cdot}O + C \rightarrow CO + S \tag{19}$$

where S is an activation site, led to the following rate expression:

$$r_c/C = \frac{k_1 P_{CO_2}}{1 + K_2 P_{CO} + K_3 P_{CO_2}} \tag{20}$$

The rate constants for the above expression for the gasification of coke are:

$$k_1 = 8.36(10)^6 \text{ Exp}(-47.7/RT) \quad (21)$$

$$K_2 = 8.48(10)^{-1} \text{ Exp}(14.9/RT) \quad (22)$$

$$K_3 = 1.3(10)^2 \text{ Exp}(6136/RT) \quad (23)$$

It can be seen from this relation that at low CO_2 partial pressures the rate expression approached first order in CO_2. At high partial pressures of CO_2 the rate expression approaches zero order. This expression also shows that the production of CO as a product inhibits the overall reaction rate.

Burnham[16,23,24] in his study of the CO_2 gasification of oil shale char under nonisothermal conditions showed that the reaction rate could best be described by two parallel reaction rates:

$$(r_c/C)_{CO_2} = .75R_1 + .25 R_2 \quad (24)$$

where $R_1 = 3.6(10)^9 \text{ Exp}(-49.0/RT) P_{CO_2}^{.2}$ (25)

and $R_2 = 9.0(10)^4 \text{ Exp}(-32.0/RT) P_{CO_2}^{.2}$ (26)

Other results from this study showed that heat pretreatment of the sample and acid leaching the samples in HCl both tended to reduce the reactivity of the char.

Steam Gasification

As mentioned previously, there is great incentive to increase the heating value of the off-gas produced during in-situ retorting. This led to some preliminary pilot plant experiments at the Laramie Energy Technology Center (LETC)[3,4] with the goal of studying the effects of O_2 and H_2O concentrations, total pressure and Fischer Assay on the heating value of the product gas. The initial experiments were conducted in a similar manner to in-situ processing in the absence of steam so that a combustion wave was caused to travel through a bed of crushed (1/8"-1/2") shale. Measurements were restricted to time varying temperature profiles in the reactor and gas chromatograph analyses of the make gas. Although these types of experiments were not conducive to kinetic

studies, the results showed a marked increase in the heating value of the make gases with moderate amounts of excess oxygen (above 21%). The effect of total pressure was interesting in that, at a constant oxygen concentration, the heating value of the make gases decreased with increasing pressures up to about 250 psi and then increased as the pressure was raised to its highest value of 545 psi. This appears to be an indication of different reactions being favored as the oxygen partial pressure changes. Since in these experiments, retorting was occurring at the same time as combutions, it is extremely difficult to isolate the various reactions which are probably occurring.

This original work was followed by a study of the effect of steam on the quality of the make gas. The same equipment and procedure was used except that steam was introduced to the reactor 15 minutes after the injection of air. Thus it is probable that the steam reacted with the carbon residue left behind by the combustion wave. Again the results were gratifying in that the run times were lowered significantly by the addition of the steam (definite proof that gasification of the carbon residue was taking place) and up to 84% of the Fischer Assay was recovered in the oil and gas. Again, however, it was not possible to study the associated kinetics although the effects of total pressure and H_2O concentration indicate that different reactions probably occur as these variables are altered.

As might be expected there is a voluminous quantity of literature dealing with the various reactions of oxygen and steam with coal. It would serve no useful purpose to review even a small portion of these works but some of the results pertain directly to oil shale, if only in a qualitative manner.

First of all it is generally accepted that the reactions of oxygen and carbon are fast under most conditions so that overall rates are often governed by heat or mass transfer limitations[25]. Dockter's[1] experience with oil-shale carbon residue is a case in point since he concluded that ash diffusion was the rate limiting step. The same is not true however for reactions of steam

and carbon or, for that matter, for any of the other reactions which might occur. The most common reactions involving steam are:

$$C + H_2O = CO + H_2 \quad (27)$$

$$CO + H_2O = CO_2 + H_2 \quad (28)$$

Reaction (27) is usually assumed to be the prevalent gasification reaction and was used by Burwell and Jacobsen[4] to determine the maximum quantity of H_2O needed in their gasification experiments. Reaction (28) is the conventional water-gas shift reaction and there was some early evidence that it could be catalyzed by components present in oil shale.

It would be expected that for coal, the rates of the reactions listed above would not be significant until temperatures become on the order of 1000 C or greater. Of course if oxidation is also occurring, then the carbon surface temperatures could easily reach those values. In any case, a great number of investigators have reported that the presence (or addition) of various alkali carbonates have a dramatic catalytic effect on all three reactions, particularly at lower temperatures (< 700 C). For example, Lewis et al[27] reported that the addition of 10% K_2CO_3 produced signficant gasification rates of wood charcoal even at temperatures as low as 700 C. They also found that the water gas shift reaction was always in equilibrium. Similar results with various inorganic additives were also obtained by many other investigators[28,31], including one investigation at pressures as high as 300 psig[32]. Of particular significance to oil-shale processing is that, in this latter study, dolomite was found to catalyze the gasification reaction(s). In a very early study, Taylor and Neville[33] showed that both potassium and sodium carbonate acted to catalyze both the water gas shift reaction and CO_2 gasification (Eq. 17) and hypothesized that the increased gasification rates were, in actuality, primarily due to the catalysis of CO_2 gasification.

Up until recently the only kinetic studies conducted on the carbon-steam reaction dealt with the steam gasification of coal. However there is

one significant difference between coal and oil shale char and that is the carbon concentration. For example it is commonly agreed upon that as coal carbon is consumed, the active surface area first increases and then decreases. This is due to the fact that carbon is the overwhelming constituent of coal. This is not the case with oil shale char however since the organic carbon content of retorted shale is at most only 8-9% by weight. When oil shale char is consumed, the shale matrix is largely unaffected; that is, barring significant mineral reactions.

Thus there have been a number of kinetic expressions proposed for the steam gasification of coal which account for the change in active surface area[34,35]. Smoot and Pratt[18] have reported that the rate of steam gasification of coal char can be described by equation (29):

$$r_c = \frac{k_1 P_{H_2O}}{1 + K_1 P_{H_2} + K_2 P_{H_2O}} \qquad (29)$$

although they mentioned that the presence of P_{H_2} in the denominator could very well be due to the influence of the water gas shift reaction.

Prior to this work, the only reported kinetic studies on the steam gasification of oil shale char was given by Burnham[36]. In these experiments, samples weighing 0.2 to 0.3 g were first retorted to 500°C and then reacted in a sweep gas at flow rates from 300 to 1500 cc/min. Steam was generated by bubbling inert gas through a constant temperature water bath. Both isothermal and non-isothermal experiments were run and the reaction rates were determined by measuring the H_2 evolution rate. The results of this study showed that the overall reaction could best be described by two parallel reaction rates:

$$(r_c/C)_{H_2O} = .57\ R_1 + .43\ R_2 \qquad (30)$$

with $R_1 = 9.6(10)^8 \exp(-44.0/RT)\ P_{H_2O}^{.5}$ (31)

and $R_2 = 1.5(10)^5 \exp(-32.0/RT)\ P_{H_2O}^{.5}$ (32)

Gas analyses indicated that most of the CO was converted to CO_2 by the water-gas shift reaction. The study also showed that heat pretreatment of the sample tended to reduce the reactivity of the char as it did in the case of CO_2 gasification.

EXPERIMENTAL APPARATUS & PROCEDURES

Equipment

Figure 1 shows a schematic of the equipment which was used for both the retorting and the kinetic phases of the investigation and Figure 2 shows the details of the reactor. Provisions were made to introduce any one or a mixture of pre-metered gases into the reactor/retort. Steam was introduced into the reactor by metering liquid water which was supplied from a large storage tank with a helium overpressure of about 2 atmospheres. An in-line paper filter was installed in the water line just upstream of a rotameter and flow control valve. This arrangement was found to produce the minimum fluctuation in the steam flow to the reactor. The gases exited the reactor via a condenser maintained at 0°C and then a gas sample valve (GSV) prior to venting. When using the apparatus in the retort mode, the condenser served to collect the oil make but no attempt was made to obtain quantitative analyses of either the oil or the product gases. When the apparatus was used for char kinetic studies, the condenser acted to separate unreacted H_2O and the water-free overhead gases were sampled on-line with the GSV and analyzed on a Carle Model 111 H gas chromatograph. The chromatograph, capable of accurate detection of H_2 at all concentrations, was equipped with a 3.5 m Carbo-Sieve B column maintained at a constant temperature of 120C with a helium carrier gas flow rate of 20 cc/min. The gas sampling equipment was capable of sampling and storing four individual samples in order to increase the sampling rate during the initial portion of a run where the reaction rates are highest. The G.C. technique was capable of base line separation of H_2, CO, CH_4, and CO_2 over a 10-minute period.

The reactor/retort (Figure 2) was inserted into a temperature programmable furnace which was controlled by a chromel-alumel thermocouple located just below the shale sample. The furnace was capable of heating rates as high as 20°C/min. up to 550°C and of operating isothermally at temperatures

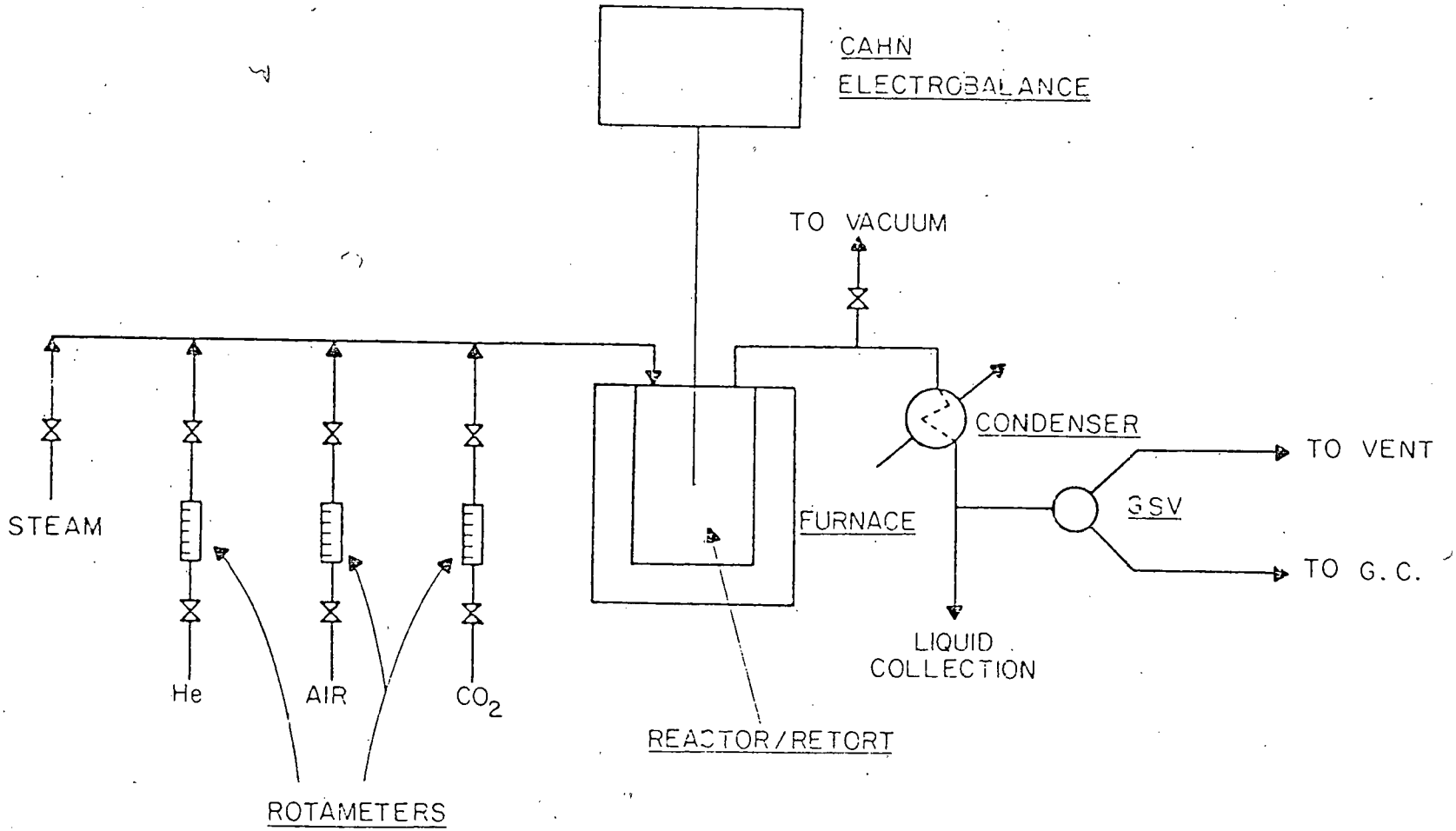

FIGURE 1: EXPERIMENTAL SCHEMATIC

FIGURE 2: REACTOR ASSEMBLY FOR KINETIC STUDIES

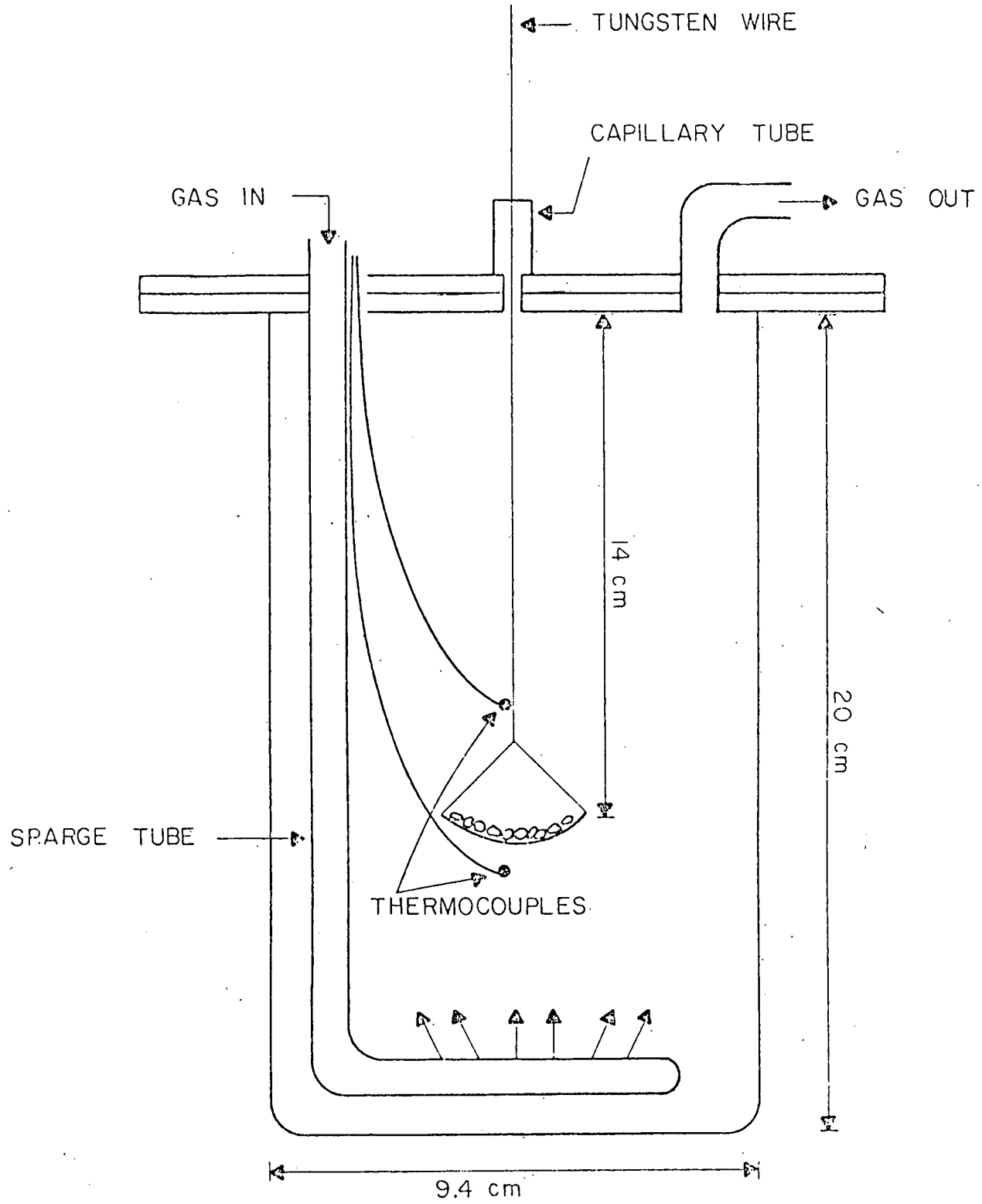

up to 870°C. When the system was used for retorting, 150 gm samples of shale (5.6-6.6 mm) were placed in a fixed bed arrangement. The carrier gas in these experiments was helium which entered at the bottom of the retort through a coiled, perforated stainless steel tube. When used for kinetic studies, 1-2 gm samples of crushed (70 microns) retorted shale were placed in a 5 cm "basket" which was in turn suspended from a Cahn Electrobalance by a 0.076 mm tungsten wire. This allowed for a continuous gravimetric measurement which was recorded on an Azar recorder. The wire exited the top of the reactor through a 2.5 cm length of 0.84 mm stainless steel capillary tubing which provided sufficient flow resistance to produce the required flow at the gas exit line (necessary for G.C. sampling). The basket itself was constructed of 400 mesh stainless steel cloth.

As mentioned previously, actual commercial operations will involve large shale pieces. In order to evaluate the simultaneous effects of chemical kinetics, gas-solid O_2 transport and O_2 diffusion through the de-charred ash layer, experiments were also run utilizing a larger tube wall furnace apparatus as shown in Figure 3. The tube had a 5 cm ID and was 1.5 m long. Separate residence time distribution studies indicated that it behaved essentially as a plug flow reactor. Here cylindrical samples were suspended in a coarse mesh stainless steel sling from a cantilevered beam equipped with strain gages. In effect this served as a large gravimetric analyzer capable of supporting the larger (2 cm diameter) shale cylinders which were employed during this phase of the study.

Procedures

Sample Preparation. The only sample preparation prior to retorting consisted of crushing the shale to uniform size ranging from 5.6 to 6.6 mm. The shale samples utilized in the study assayed between 15 and 50 GPT. After retorting, the samples were stored under a nitrogen blanket and then crushed to about 70 microns prior to utilization in the kinetic studies. In order to be able to study reaction kinetics at high temperatures without the

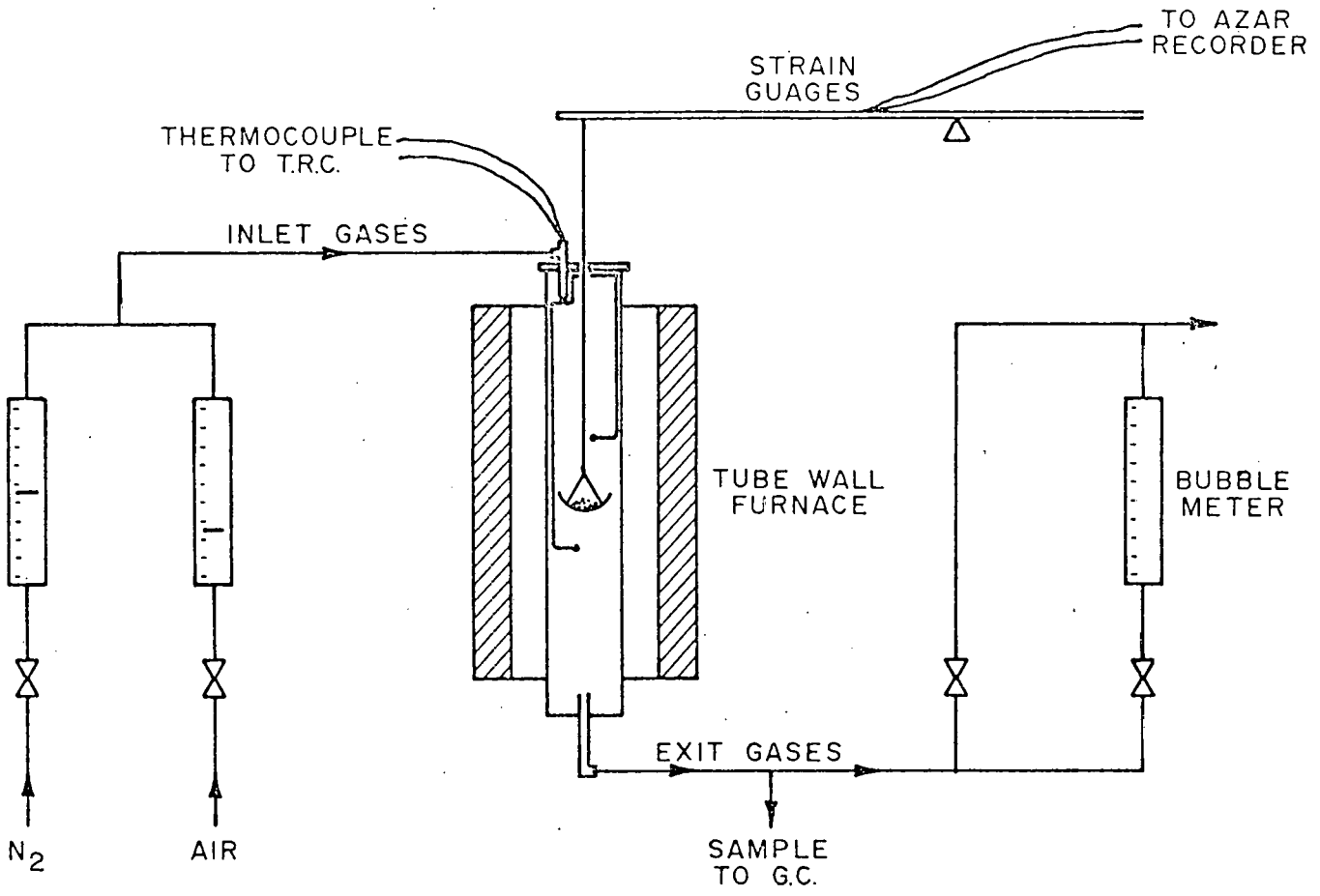

FIGURE 3: FLOW EQUIPMENT MASS TRANSFER STUDIES

added complexity of simultaneous mineral decarbonation, a number of samples were acid leached. This was done in two ways so that a separate evaluation of the presence of different mineral compounds could be obtained. Some samples were leached in a 5% H_2SO_4 solution (immersion for 10 minutes under boiling conditions) in which case insoluble sulfates were formed. Other samples were similarly leached in 5% HCl which succeeded in removing the soluble chlorides of Ca, Mg, and Fe.

The samples employed in the mass transfer studies consisted of 2 cm diameter cylindrical core samples which were cut both perpendicular and parallel to the bedding plane. A number of runs were conducted with these samples placed so that the longitudinal axis was perpendicular to the gas flow. This allowed for reasonable predictions of the velocity distribution around the sample and thus, more accurate measurements of gas-solid mass transport coefficients. This would also simulate to some extent, shale pieces which might be exposed on all sides to reacting gas media. In other experiments the procedure of Dockter[1] was utilized. That is, the cylindrical surface was wrapped with impermeable foil and the sample was placed with the longitudinal axis parallel to the flow stream. In this case it was possible to obtain effective O_2 diffusivities both perpendicular and parallel to the bedding plane and thus these data should give the maximum range of the diffusivities to be expected. Unfortunately however, there was visible evidence that the heat generated by the coring process resulted in partial fusion of the cylindrical surface.

Retorting. At room temperature the retort was first evacuated and then flushed with helium in order to remove all traces of oxygen. All retorting runs were conducted with a helium purge gas since it contained, at most, only 20 ppm O_2. The retorting was carried out at heating rates from 0.3 - 17°C/min. up to a maximum temperature of 500°C and at purge gas velocities from 4 to 40 cm/min. (500°C). A few runs were held at 500°C for up to an hour, and it was concluded that once the temperature reached this value, complete kerogen decomposition had taken place.

Isothermal Kinetic Experiments. In these experiments, the reactor was initially flushed with helium until the exit O_2 concentration dropped to the value inherent in the helium purge stream. The temperature was then raised to the desired level at which point the preselected reactant (oxygen, steam, CO_2) mixture was introduced to the reactor. Reactant concentrations were varied by dilution with helium which was preset with the reactor on bypass. With O_2 or CO_2, it typically took about 1.5 minutes before the reactor attained the inlet composition. This was due to the fact that the reactor behaved very similarly to an ideal back-mix reactor which was verified by separate step-change residence time distribution measurements. For experiments conducted with steam in the carrier gas, the steam concentration in the reactor reached the inlet concentration in about 30 seconds. This was due to the sudden expansion of the liquid H_2O as it entered the reactor.

Non-Isothermal Kinetic Experiments. A number of runs, primarily to evaluate kinetic interactions during simultaneous reactions, were conducted in a non-isothermal manner. While these experiments are not ideally suited to obtaining complex kinetic data, the primary purpose was to compare the predictions of previously determined kinetic expressions with experimental measurements.

All non-isothermal experiments were conducted using 1 gm retorted shale samples. The samples were first heated to 400C in helium to remove moisture and to stabilize the low temperature decomposition reactions (dawsonite and nahcolite). At this point the desired sweep gas composition was introduced and the reactor temperature was raised at about 2 C/min to a maximum temperature of about 800C. At the end of each of these runs the sample was decharred in air (to determine the quantity of char remaining), decarbonated in helium (to determine residual $CaCO_3$), and then recarbonated at 600C in a He/CO_2 mixture (to determine total CaO make during the run).

Mass Transfer Measurements. As stated previously, gas-solid and diffusional mass transport of oxygen was studied using 2 cm cylindrical core

samples in the large tube furnace shown in Figure 3. Because of the size and mass of these samples it was necessary to restrict these measurements to shales which assayed at 20 GPT or less. If assays much exceeded this value, there was a high risk of the loss of the structural integrity of the sample during retorting. The raw shale sample was placed in the desired position (parallel or cross flow orientation) within the furnace and, after a one-hour helium purge, was retorted at 475C in a helium purge of 1 cm/sec (475C). These conditions were maintained until the gravimetric measurements indicated that retorting was complete, usually about two hours. The sample was then cooled to room temperature at which point the gravimetric analyzer was re-calibrated and the sample was carefully re-positioned in the sling. The temperature was then raised to the desired value in helium when the preselected air-helium mixture was introduced to the reactor. Superficial gas velocities were varied from 0.5 to 4.0 cm/sec which corresponded to particle Reynolds numbers from 2 to 16.

RESULTS

Effect of Retorting on Char-Make

Table 1 shows the results of the retorting experiments in terms of the percentage of the weight of the raw shale which is lost during retorting. The replicates at the high retorting rate show that the repeatability was typically within about 2%. From these data it appears that higher purge velocities consistently produce larger weight losses. Table 2 shows the results in terms of the char quantity (% raw shale) and here the trends are more distinct although the data scatter is larger.

In analyzing these results distinction must be made between those samples retorted at a low velocity (4 cm/min) and those at a high velocity (40 cm/min). Thus, at low purge velocities, low retorting rates produce a larger quantity of char. Presumably this occurs due to the prevalence of pyrolysis reactions which form carbon precursor compounds at low retorting rates. The fact that the purge velocity is so low increases the probability that product cracking will occur before the products can be removed from the system. This can also be seen from the results obtained at a low retorting rate when the purge velocity was increased. That is, with the exception of the one run (asterisk in Table 2), increasing the purge velocity resulted in a lower organic carbon residue which is consistent with the above explanation. The implication of these results for proposed commercial processing is not significant, however. Surface retorts typically operate at high retorting rates and here there is no effect of purge velocity. Although in-situ processing takes place at low retorting rates, it is doubtful whether the purge velocities would ever be low enough where this could be a problem.

The quality of the char was evaluated by examining its chemical reactivity. This was accomplished by exposing the retorted samples to air and noting the temperature at which oxidation was initiated while the temperature was being raised at 15 C/min. These experiments indicated that, with the exception of the char produced at 3°C/min. and a 4.0 cm/min purge velocity, there were no significant differences in this oxidation "light-off" temperature. A second set of experiments was also conducted to examine char reactivity. These experiments attempted to evaluate the hydrogenation capability of the residue

TABLE 1

WEIGHT LOSS DURING RETORTING

(% of Raw Shale)

Retorting Rate → / Purge Velocity[a] ↓	0.3°C/Min	17°C/Min Replicates		
4.0 cm/min	9.22	9.31	9.39	15 GPT
40.0 cm/min	9.86	9.85	9.75	
4.0 cm/min	14.78	16.25	15.33	30 GPT
40.0 cm/min	16.06	16.73	16.40	
4.0 cm/min	24.43	24.70	25.05	50 GPT
40.0 cm/min	25.08	25.87	25.44	

[a] Velocities at 500 C, 1 atm.

TABLE II

CHAR QUANTITY AFTER RETORTING

(% of Raw Shale)

Retorting Rate → / Purge Velocity[a] ↓	0.3°C/Min	17°C/Min Replicates		
4.0 cm/min	3.06	2.56	2.22	15 GPT
40.0 cm/min	2.35	2.34	2.18	
4.0 cm/min	5.11	4.03	4.63	30 GPT
40.0 cm/min	5.21*	4.25	3.71	
4.0 cm/min	7.26	5.73	4.64	50 GPT
40.0 cm/min	5.19	5.35	4.61	

[a] Velocities at 50 C, 1 atm.

* Suspicious Data

by exposing it to hydrogen. Activity was measured in terms of the temperature at which methane first appeared in the exit gas. Again, it was found that all of the retorted samples began to produce methane at about the same temperature (475°C) and thus it was concluded that the differences in the retorting parameters did not affect the quality (reactivity) of the char produced. As will be discussed below, the reactivity of the char produced at the lowest purge gas velocity and retorting rate was markedly lower. This is probably due to product cracking which produces a more inactive char as concluded by Stout et. al.[10]

Oxidation Kinetics

Since the stated goal was to obtain kinetic data in the absence of mass transfer effects, it was important to ensure that neither gas-solid nor internal diffusion were rate limiting factors. The former was checked by measuring the oxidation rates at 550°C and .075 atm oxygen at different gas flow rates and the results are shown in Figure 4. Since there was no increase in the fraction of char oxidized (x) as the flow rate was doubled from 400 to 800 scc/min it was concluded that the experiments were free of significant gas-solid mass transfer resistances. However this is only a valid conclusion with respect to convective transport phenomena which is dependent on flow rates. As will be discussed in more detail below, additional measurements of the actual sample temperatures indicated that radiative energy transport was a significant factor in maintaining near isothermal conditions at the initiation of the exothermic oxidation reaction. In addition, oxidation reaction rates were faster at higher O_2 pressures and there was definite evidence of significant gas-solid mass transport resistance at temperatures greater than 550 C. However, in order to obtain accurate gravimetric measurements, it was necessary to restrict the gas flow rates to about 650 scc/min and this value was subsequently used for all the experiments reported here.

Internal diffusion phenomena has already been mentioned as the rate limiting factor in previous work[1,22] but those investigations were all conducted with relatively large sample pieces. Even with the small particle sizes used here (70 μm), ash diffusion can still be a problem since char oxidation is a relatively rapid reaction. If this were the case, the problem would be most severe near the end of a run when most of the unoxidized char

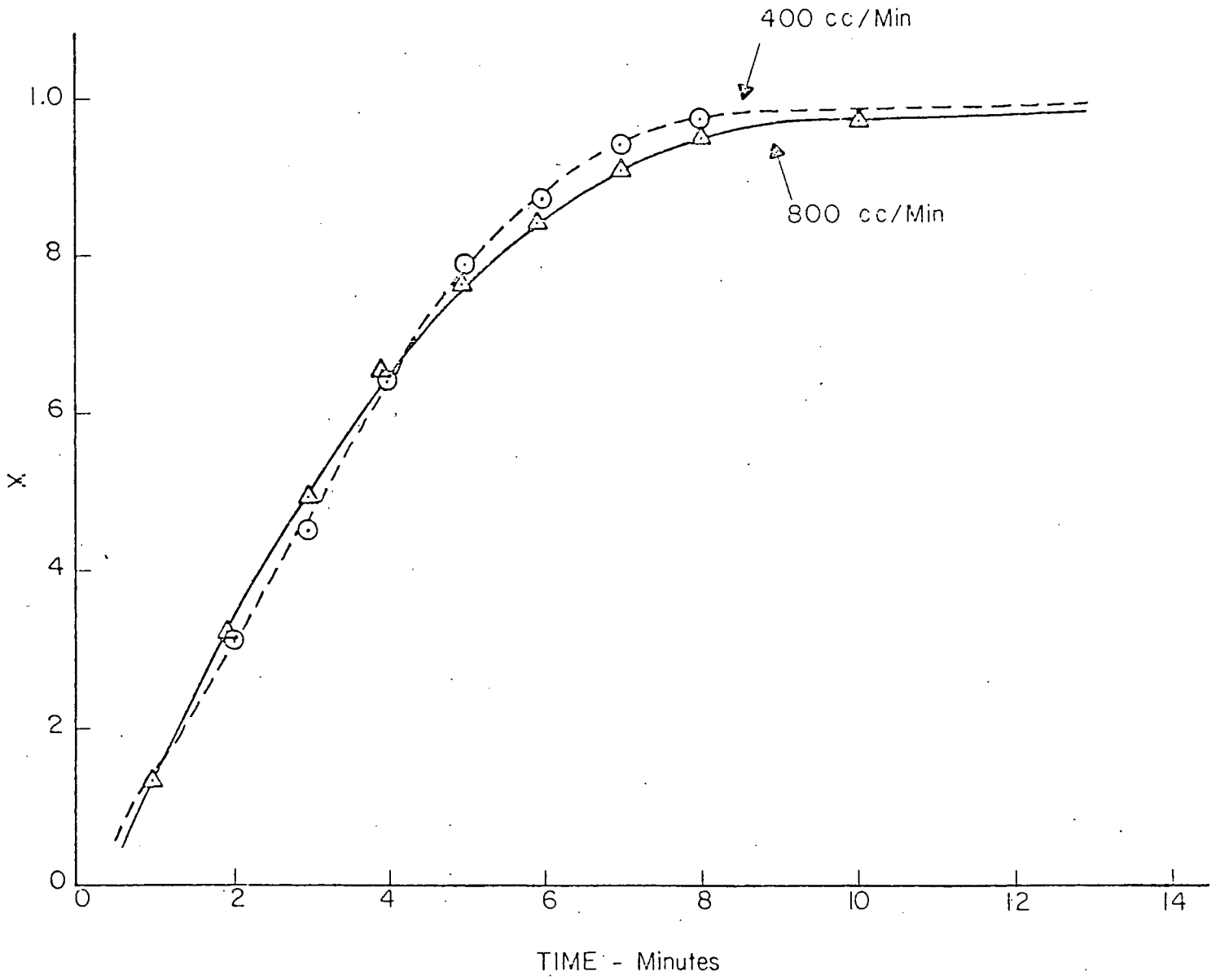

FIGURE 4: EFFECT OF GAS FLOW ON CHAR OXIDATION RATE

would be located near the center of the particle. This was evaluated in a few selected runs by raising the temperature after 90% of the char had been oxidized. As can be seen from Figure 5, the conversion rate increased dramatically as soon as the temperature was increased. This is clearly indicative of a chemical reaction rate as opposed to a temperature insensitive diffusion rate. Thus it can be concluded that the kinetic data reported here were free from any diffusional effects.

The kinetic data were all correlated in terms of the fraction of the char converted and, in an unsteady state experiment such as this, the oxidation reaction rate might be expected to take the empirical form

$$C_0 \frac{dx}{dt} = k_0 \exp\left[\frac{-E^*}{RT}\right] C_0^{\alpha}(1-x)^{\alpha} P_{O_2}^{\beta} \qquad (33)$$

where C_0 is the initial char concentration (gm/gm of shale), E^* is the activation energy, P_{O_2} is the oxygen partial pressure (atm), T is the temperature (°K) and α and β are the reaction orders with respect to the residue and oxygen.

Although the experiments were designed to run at a constant oxygen concentration, this was not possible for runs where significant char consumption occurred during the first 2-3 minutes after oxygen exposure. This is due to the fact that it took a finite time for the oxygen mixture to displace the helium in the reactor. In order to obtain a quantitative evaluation of this phenomenon, experiments were conducted in which the exit concentration of a tracer gas was monitored as a function of time following a "step-change" in the feed gas. Figure 6 shows such a plot and the data correspond closely to an ideally mixed reactor; one where the exit concentration is identical to the concentration within the reactor. In terms of oxygen then, its variation with time for a constant feed pressure $\left(P_{O_2}\right)^o$ is

$$\frac{P_{O_2}}{\left(P_{O_2}\right)^o} = 1 - \exp\left[-t/\bar{t}\right] \qquad (34)$$

where $\bar{t}$ is the average residence time in the reactor.

The kinetic data were evaluated using integral analysis techniques[37]. Thus, if the oxidation rate is assumed to be first order with respect to both the residue (α =1) and oxygen (β = 1), equation (33) can be integrated upon the substitution of equation (34) for P_{O_2}. This results in

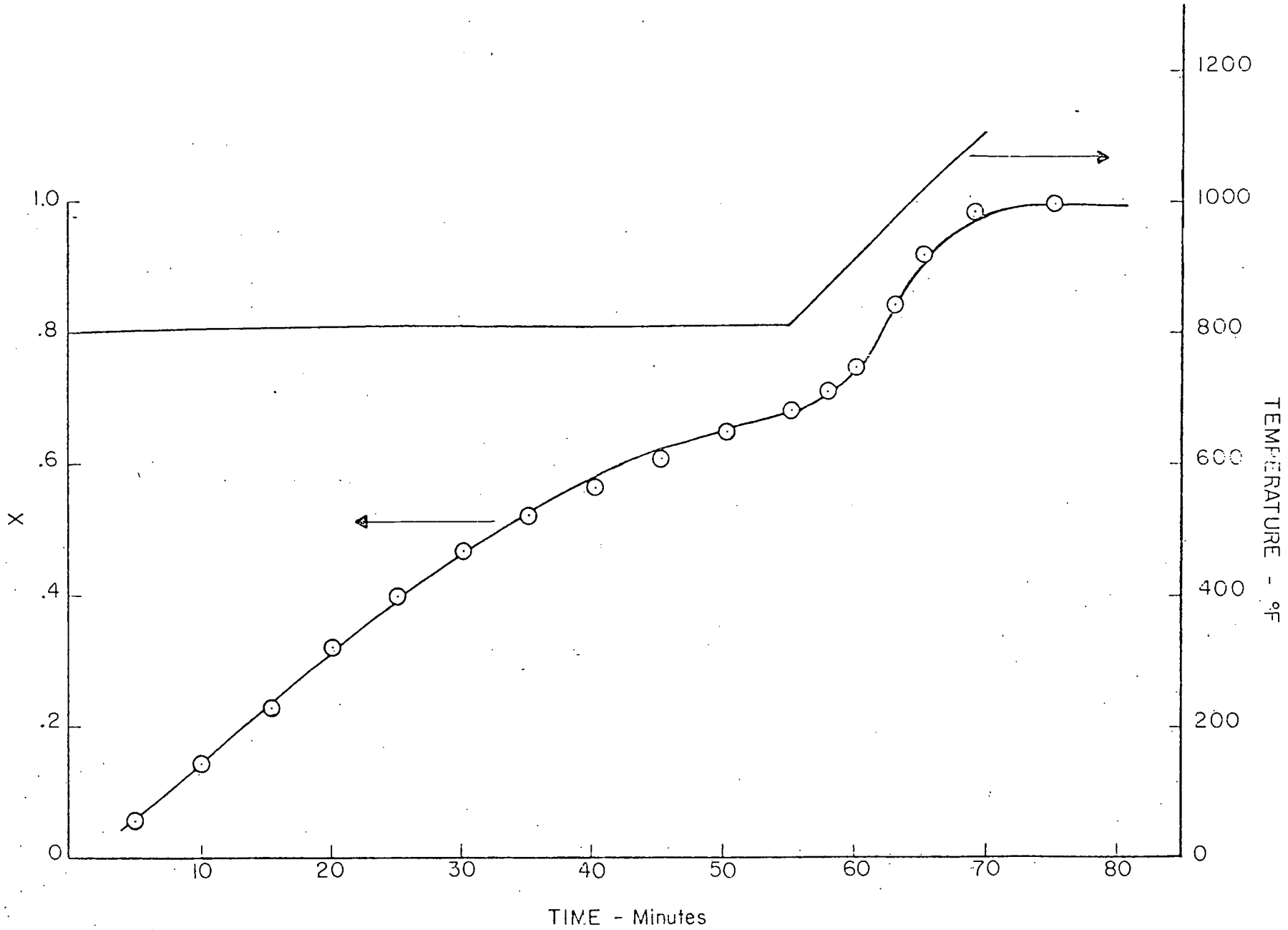

FIGURE 5: RESPONSE OF CHAR CONVERSION TO TEMPERATURE CHANGE AT END OF RUN

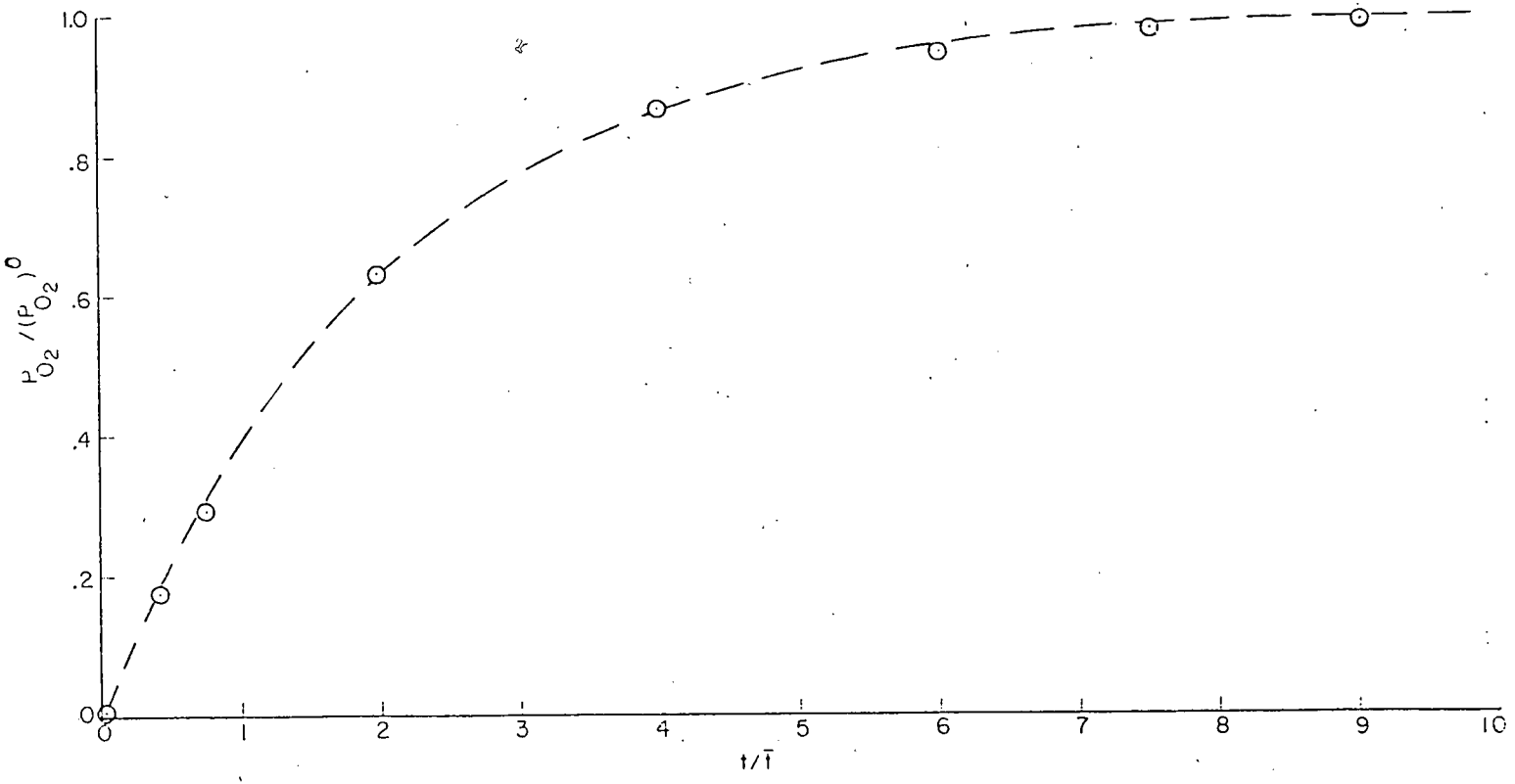

FIGURE 6: RTD ANALYSIS OF REACTOR FOLLOWING STEP CHANGE

$$\ln(1 - x) = -k^*F(t) \qquad (35)$$

where

$$k^* = k_0(P_{O_2})^0 \exp\left[\frac{-E^*}{RT}\right] \qquad (36)$$

$$F(t) = t - \bar{t}\left(1 - \exp\left[\frac{-t}{\bar{t}}\right]\right) \qquad (37)$$

When the data were analyzed in this manner the results were found to be very repeatable; within three percent for two experiments conducted under the same conditions two weeks apart. It was also possible to evaluate the char consumption rate for some runs by analyzing the exit gases. In all cases, CO_2 was the only combustion product detected in the exit gas. Since hydrogen is also expected to be present in the residue and it was not possible to detect H_2O in the exit gas, the difference between the weight loss measured by the gravimetric technique and that accounted for by the CO_2 carbon was attributed to hydrogen oxidation. It was only possible to do this however, for runs with relatively slow oxidation rates since the maximum G.C. sampling rate was one sample/four min. The results for these runs indicated that the C/H ratio was approximately 1.5.

Oxidation Reaction Orders

The first set of oxidation experiments were conducted with shale samples with their mineral carbonates intact. To do this of course, required that the experiments be conducted at temperatures below 600 C. Figure 7 shows the results of a first order analysis plotted according to equations (35) and (37) at 425 C for various O_2 partial pressures with a 50 GPT shale sample. As can be seen, good first order plots are obtained at all O_2 pressures which is a clear indication that char oxidation is first order with respect to the char present. As indicated by equation (36), the slopes of these lines are equal to k* which should plot linearly with P_{O_2} if oxidation is first order with respect to O_2. That this is indeed the case can be seen from Figure 8 where all but the very low P_{O_2} runs fall on the first order line. The deviation at low P_{O_2} is attributed to the difficulty in controlling the low O_2 flow rates at these conditions. Note also that the results for 15 and 50 GPT shales were all the same, indicating that there is no separate influence of the shale assay. Because of this, all subsequent experiments were conducted with 50 GPT shale since it produced a higher concentration of char and consequently gave more accurate and reproducible results.

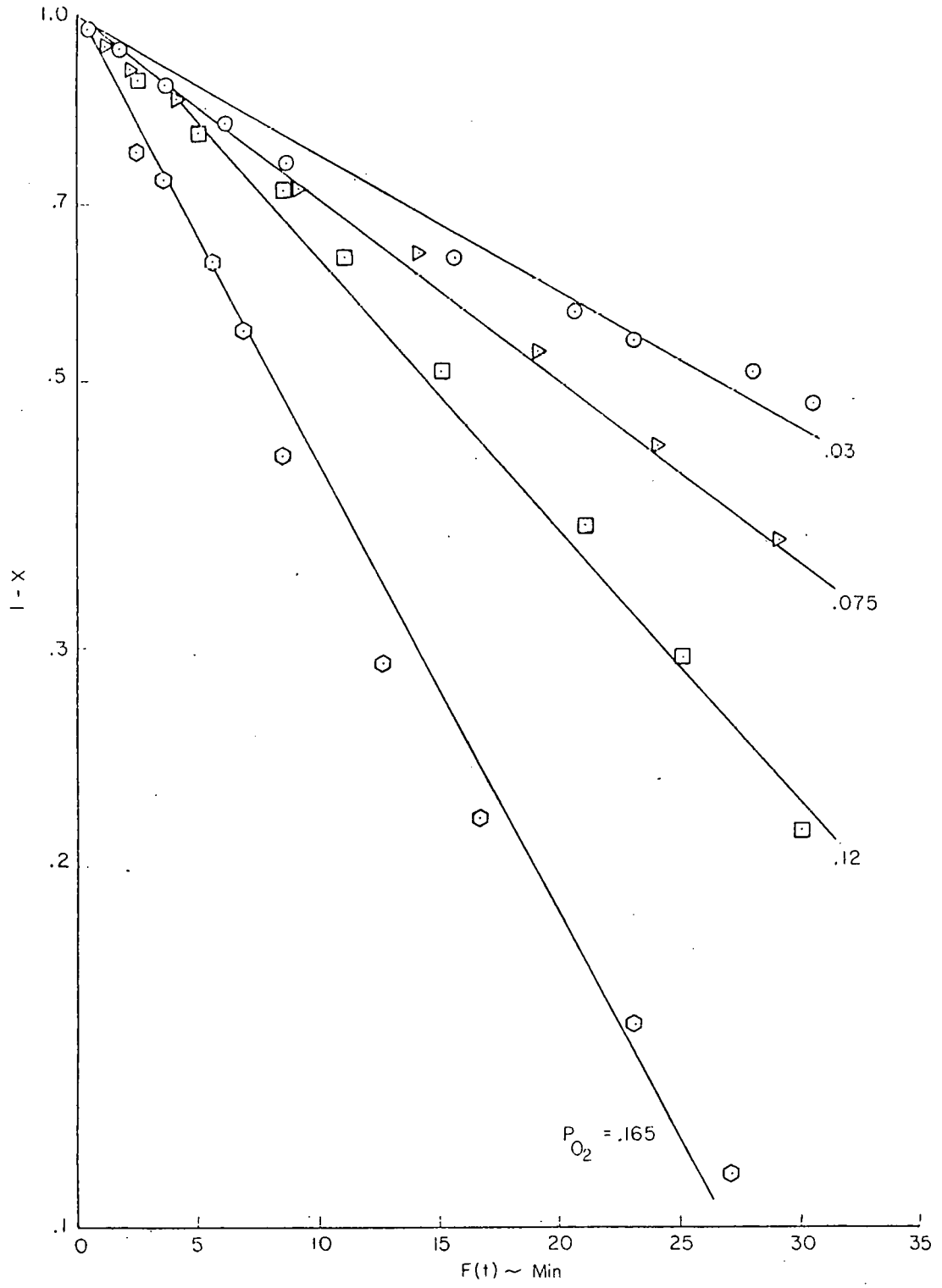

FIGURE 7: CHAR OXIDATION - FIRST ORDER PLOTS AT 425°C

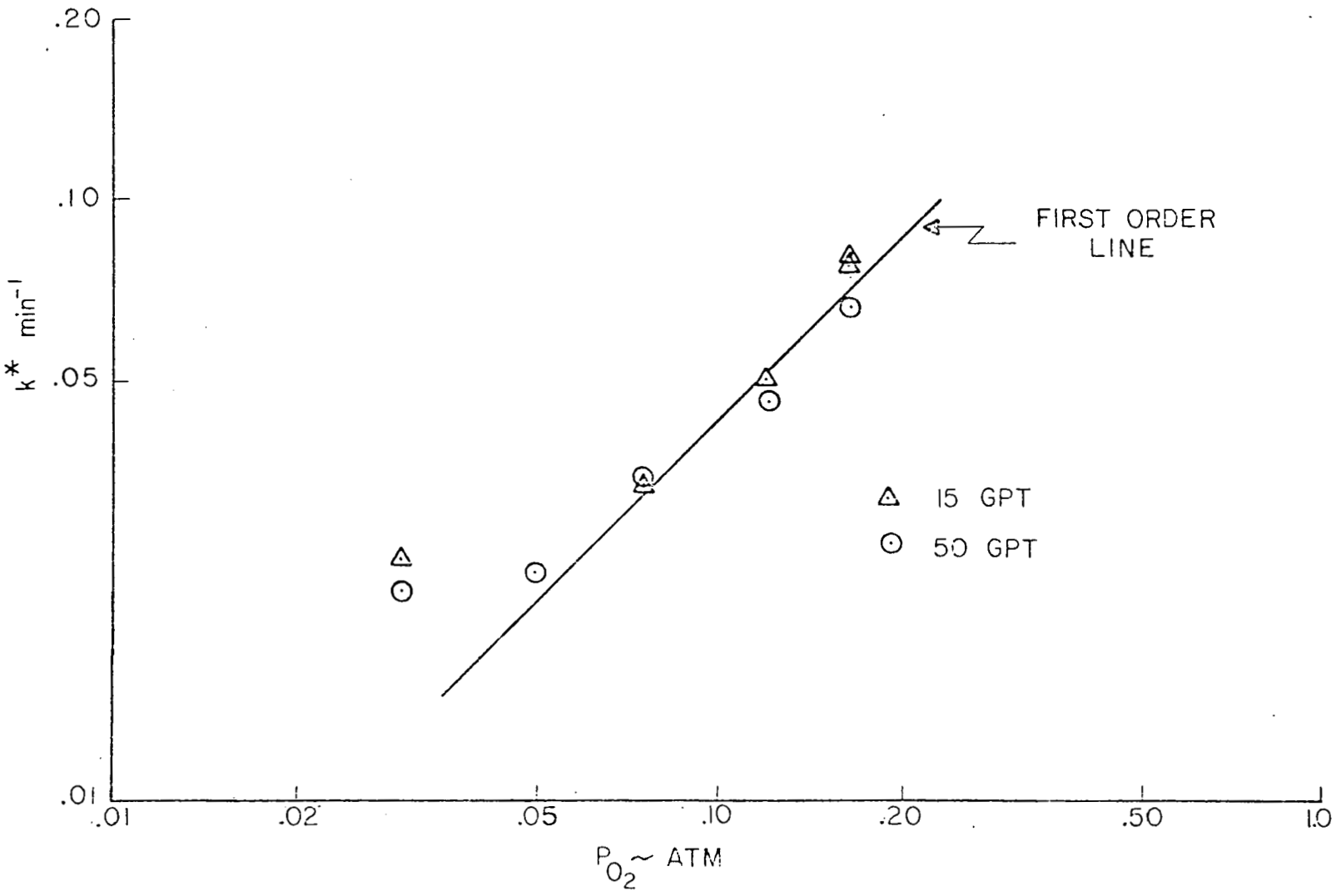

FIGURE 8: ANALYSIS OF OXIDATION REACTION ORDER (425 C)

Figure 9 shows first order plots for two temperatures at P_{O_2} = .075 atmospheres. While a good first order plot is obtained at the lower temperature, the high conversion data at 572 C (845 K) lie below the apparent first order line. Deviations similar to these were found at all runs conducted at temperatures greater than 550 C and could be attributed to gas-solid mass transport effects, as will be discussed below.

Oxidation of Slow Retorted/Acid Leached Shale

In the previous section it was pointed out that shale retorted at 0.3°C/min. and in a purge gas velocity of 4 cm/min, "slow retorted" shale, produced a larger quantity of char. The reactivity of this same char was also evaluated by comparing its rate of oxidation with the rates measured for fast retorted shale. As shown in Figure 10, the slopes of the first order plots for the slow retorted shale are about 40% lower than those for the fast retorted shale at both temperatures. Since P_{O_2} was the same in these runs (0.075 atm), this means that the rate constants for slow retorted shale are also 40% lower. Since the low char reactivity is attributed to coke formed from the cracking of the product oil, it is highly probable that char produced within large blocks of shale, such as would be present in In-Situ retorting, may also have a significantly lower reactivity. This hypothesis, however, has not been tested as of yet.

The reasons for acid leaching of the shale samples have already been given during the discussion of sample preparation. The oxidation rate constants for acid leached shale, whether HCl or H_2SO_4 leached, were found to be essentially the same as those for shale with its mineral carbonates intact. This is shown in Figure 11 which is an Arrhenius plot corresponding to a temperature range of 425-700 C. It should be pointed out that the temperatures corresponding to the data points in Figure 11 are average values for the particular run. Separate measurements of the shale sample temperatures indicated that upon initial exposure to oxygen the sample experienced a temperature rise of about 25 C and then cooled to the original bulk gas temperature. Interestingly, a major fraction of the cooling mechanism was found to be radiation from the small shale sample to the relatively large reactor surfaces. The activation energy corresponding to the straight line through the data points is 23,200 cal/mole. The straight line was drawn to give greater weight

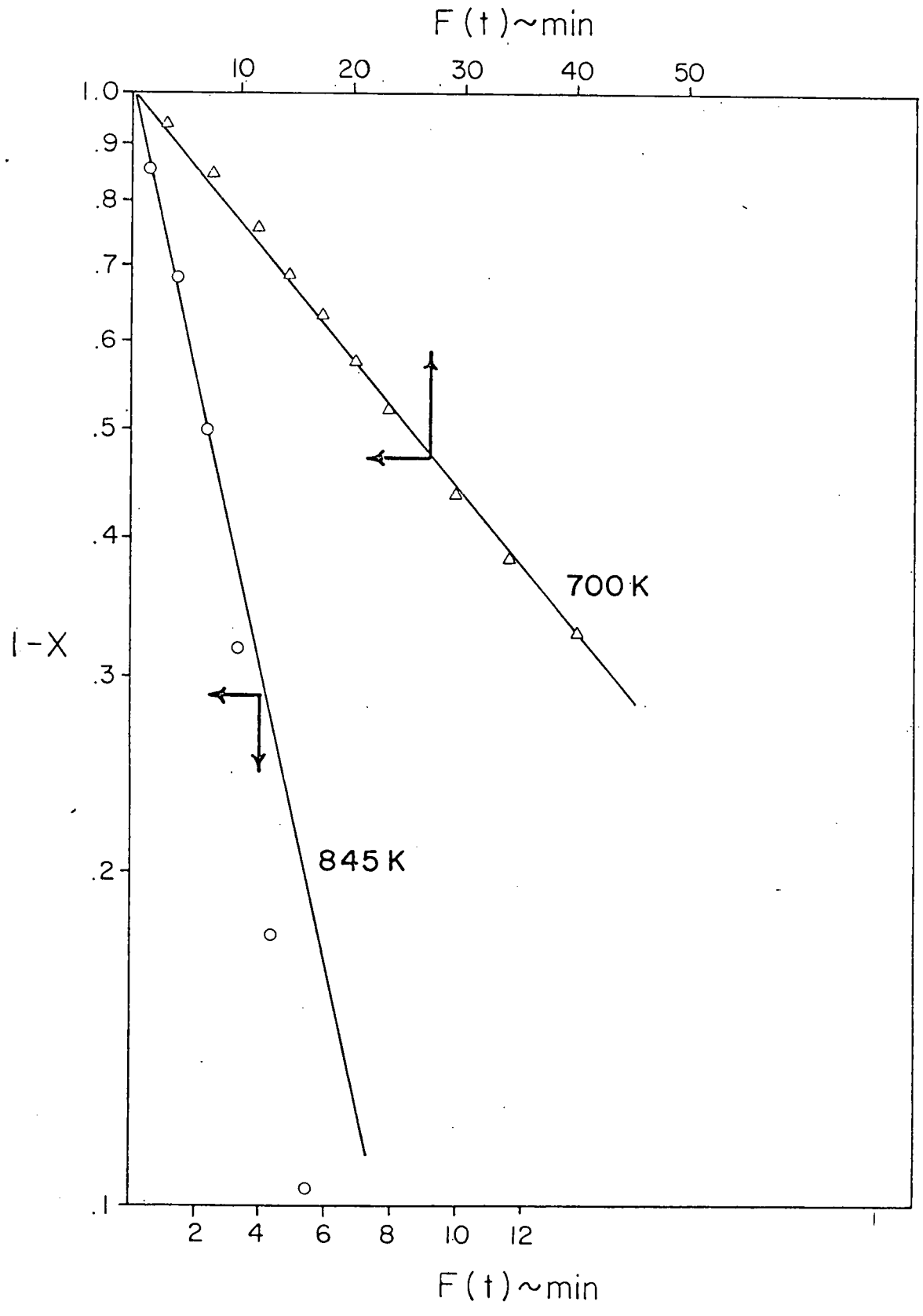

FIGURE 9: FIRST ORDER OXIDATION PLOT AT TWO TEMPERATURES (P_{O_2} = .075 atm)

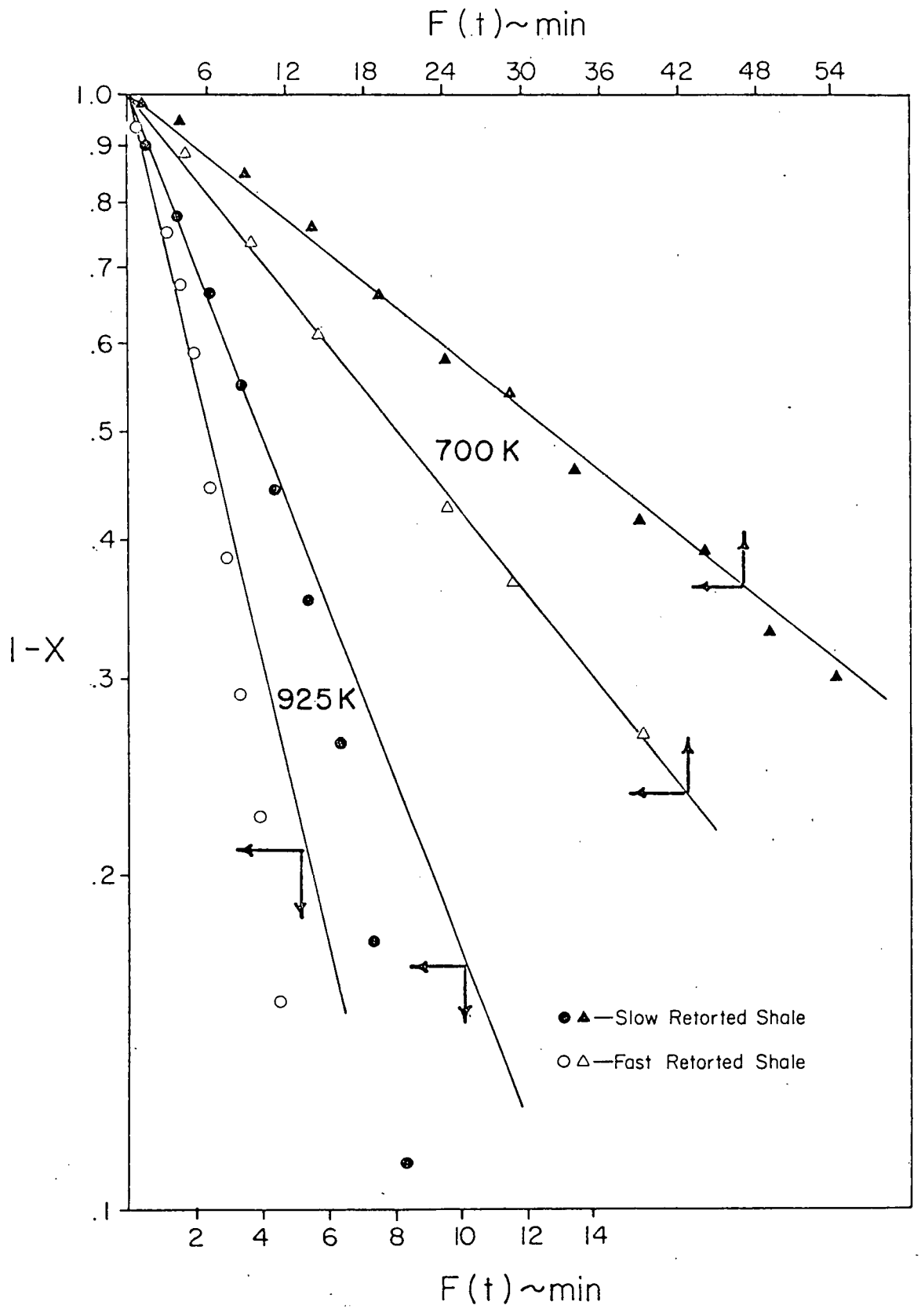

FIGURE 10: COMPARATIVE OXIDATION FOR SLOW RETORTED SHALE (P_{O_2} = .075 atm)

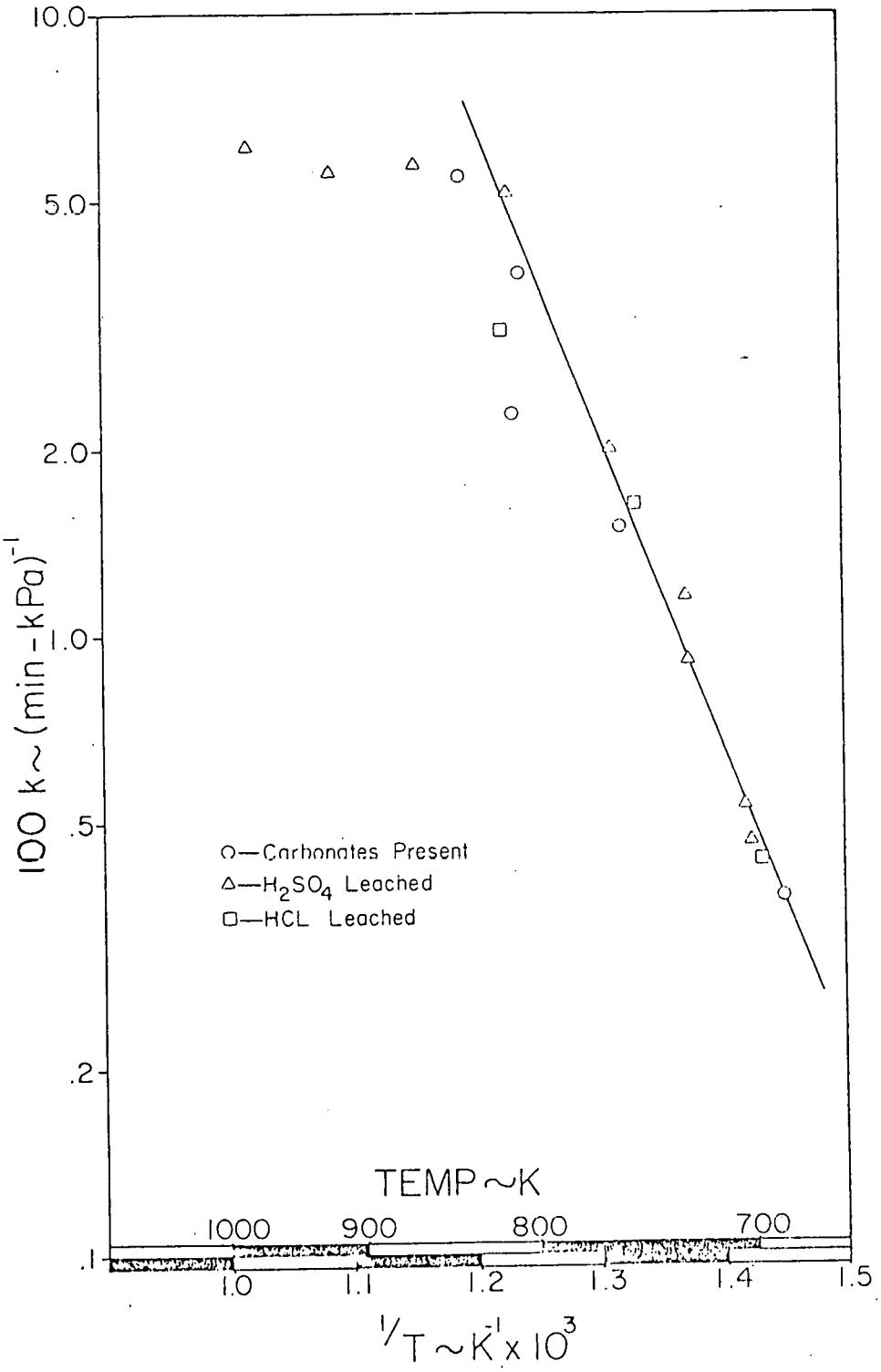

FIGURE 11: ARRHENIUS PLOT FOR CHAR OXIDATION

to the low temperature data since the high rates at high temperatures are thought to be less accurate due to the relatively short run times. The fact that the temperature dependency of the high temperature rate constants is almost negligible indicates that the oxidation rate is being influenced by mass transport rate limitations. Since internal diffusion had already been found to be insignificant, mass transport influences are most assuredly due to gas-solid transport. A more detailed analysis of this will be presented in the discussion of oxygen mass transport during char oxidation.

Oxidation of Thermally Decarbonated Shale

The problems of mineral decomposition have already been thoroughly discussed in the BACKGROUND section of this report. In actual retorting processes, whether surface or in-situ, it is most likely that at least some of the char oxidation will occur simultaneously with mineral decomposition. Since in this case the shale will see various CO_2 concentrations, the extent to which calcite will decompose to CaO is uncertain. In order to evaluate the effect of the presence of CaO on char oxidation, it was decided to examine the extreme case in which all of the calcite was decomposed to CaO.

Prior to oxidation the samples were raised to temperatures on the order of 675 C in the presence of inert helium and maintained at this temperature until all the dolomite and calcite had decomposed to the oxides. This was verified by both continuous gravimetric readings and G.C. analyses of the exit gas. It should be pointed out that during this procedure approximately 10% of the char ($\sim$ 5 mg) reacted with the CO_2 produced during mineral decomposition to produce CO (detected by gas chromatography). The fact that this reaction occurred to such an extent even though the measured CO_2 partial pressure never exceeded 0.01 atmospheres, is an indication of the surface active nature of CO_2 gasification. That is, the CO_2 released by mineral decomposition is readily accessible to the char and the reaction evidently proceeds at a much faster rate than would be measured if the CO_2 had to be supplied by the bulk sweep gas.

Figure 12 shows the raw gravimetric data for two runs conducted with thermally decarbonated shale, one at 700 K and the other at 945 K. It is interesting that in both cases the sample weight initially *increases* as char oxidation begins. Even more interesting is the fact that the weight increase

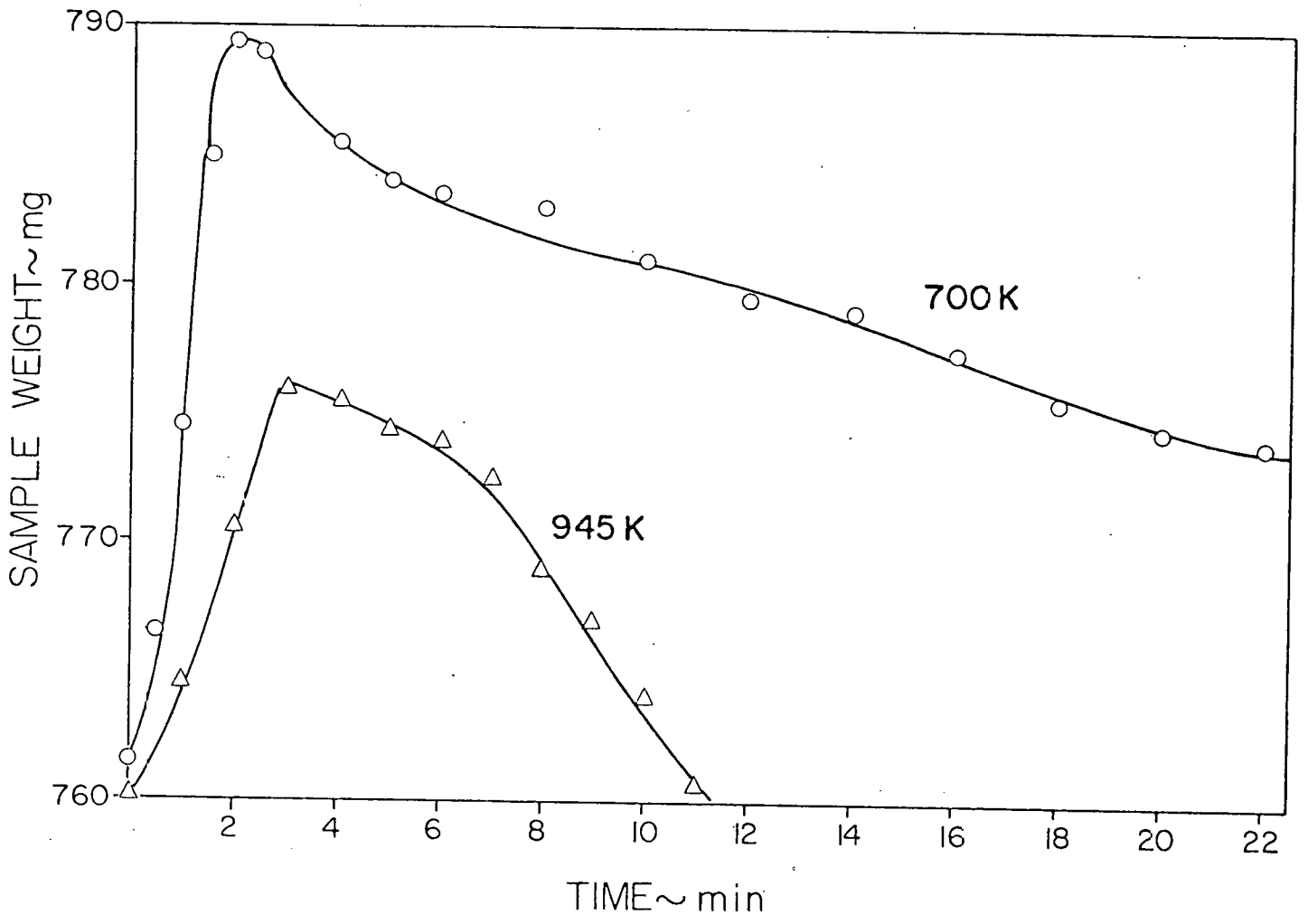

FIGURE 12: SAMPLE WEIGHT CHANGES DURING OXIDATION OF THERMALLY DECARBONATED SHALE (P_{O_2} = .075 atm)

is higher at the lower temperature. Evidently the CaO present in the sample is recombining with the CO_2 produced by char oxidation to reform the carbonate ($CaO + CO_2 \rightarrow CaCO_3$) since this is the only mineral reaction which is reversible. Not only does this account for the initial weight increase but also for the larger weight increase at the lower temperature. This latter effect is apparently due to equilibrium considerations since lower temperatures favor carbonate reformation, at least from a thermodynamic point of view. It should also be pointed out that the temperatures indicated in this figure are temperatures in the bulk gas stream. At these temperatures thermodynamic equilibrium for the carbonate decomposition reactions would not be expected. Separate experiments were therefore conducted to obtain measurements of the actual shale temperatures during oxidation. Unfortunately, due to the sensitivity of the electrobalance it was not possible to obtain simultaneous weight measurements. Nevertheless, these experiments indicated that, in these two runs, the shale temperatures reached maximum values of 775 K and 975 K at very nearly the same time as the observed maximum in the sample weight.

Another factor of importance is that the carbonate reformation reaction can only occur as fast as the char oxidation reaction since the CO_2 required for the carbonate reaction is supplied by char oxidation. Thus the rate of weight increase indicated in Figure 12 provides a lower estimate of the char oxidation rate. When this analysis was conducted, it was found that the char oxidation rate was at least an order of magnitude greater than that observed when the minerals were left intact. These results then prompted a dynamic mathematical simulation to predict the sample weight as a function of time. This was accomplished by solving the differential equations which described the rates of char oxidation, calcite recarbonation and species consumption/production within the CSTR, using the IBM CSMP program. The pre-exponential factors for the char oxidation rate constant obtained earlier (Figure 11) and for the rate of calcite recarbonation (obtained in separate experiments and discussed below) were systematically adjusted until reasonable matches were obtained to the data shown in Figure 12. The best match was obtained with a char oxidation rate constant equal to ten times the values given in Figure 11. Furthermore, using the measured shale temperatures for both runs, the simulation indicated that at the maximum sample weights shown in Figure 12, the rate of recarbonation was very nearly zero (close to equilibrium) and

approximately 10-25% of the char remained. Thus the weight loss which occurs after the maximum is reached is due to the consumption of the remaining char. Another interesting result from the simulation was that the calcite recarbonation rate was also significantly higher in these experiments (∿ 2 orders of magnitude) than when CO_2 is supplied by the bulk sweep gas. This would indicate the possibility that char oxidation is being catalyzed as a result of the thermal decarbonation procedure. There are at least three possibilities for these effects: (1) increased pore volume due to the original decarbonation; (2) the iron contained one of the shale minerals, ankerite, (∿ 1.5%) is an oxidation catalyst or; (3) the oxides produced by carbonate decomposition are oxidation catalysts. While it is difficult to prove any of these conclusively, there is evidence to support the rejection of the first two possibilities. That is, since leaching with HCl resulted in the same oxidation rate as unleached shale despite a three fold increase in available surface area[38], it would seem that the explanation does not lie here. Furthermore, HCl-leached shale should not contain iron and this iron-free shale had the same oxidation activity as that containing iron. Thus a definite possibility is that the oxides produced during thermal decomposition catlayze the char oxidation. In fact CaO is a known catalyst for a number of reactions[39]

Both MgO and CaO are produced during thermal decarbonation, the former by dolomite decomposition, the latter by calcite decomposition. Chemisorption experiments were conducted at 25 C in order to evaluate the capability of thermally decarbonated shale to adsorb O_2 and CO_2. Table 3 shows the results and as can be seen there is definite indication of O_2 chemisorption on the decarbonated shale and a dramatic increase in the CO_2 uptake over

TABLE 3

O_2 AND CO_2 ADSORPTION MEASUREMENTS ON RETORTED OIL SHLAE (25 C)

SAMPLE	O_2 UPTAKE[a]	CO_2 UPTAKE[a]
Thermally Decarbonated	15	125
Carbonates Present	∿0	25

[a] μmoles/gm sample

that measured with carbonates present. However it should be pointed out that while the O_2 isotherm was similar to that expected for chemisorption (shallow slope), the dependency of CO_2 uptake on pressure was more significant and the possibility of some physical adsorption taking place cannot be ruled out.

The fact that the carbonate reformation rate was also much higher when CO_2 is supplied by char oxidation, is an indication that a surface active step might be part of the reaction mechanism. This is supported by the relatively high CO_2 adsoprtion capacity of thermally decarbonated shale (Table 3). Given this, together with the demonstrated capability for oxygen chemisorption to occur, the following mechanism is hypothesized:

$$O_2 + CaO \leftrightarrow O_2 \cdot CaO \quad (38)$$

$$O_2 \cdot CaO + C \rightarrow CO_2 \cdot CaO \quad (39)$$

$$CO_2 \cdot CaO \rightarrow CaO + CO_2 \quad (40)$$

$$CO_2 \cdot CaO \leftrightarrow CaCO_3 \quad (41)$$

where X·Y indicates that X is chemisorbed to Y. Equations (38) and (39) could explain the oxidation catlaysis and equations (40) and (41) are competitive reactions which determine the extent of carbonate reformation. This would also explain the increased rate of carbonate formation during char oxidation; i.e., the CO_2 does not have to adsorb [via the reverse of reaction (40)] since it is produced in an adsorbed state by means of reaction (39).

Reaction Rate Expression For Char Oxidation

All of the kinetic oxidation data obtained with shale which had not been thermally decarbonated were consistent up to a temperature of 550 C. Above this temperature significant gas-solid mass transport resistances were evident. As discussed above, there is strong evidence of catalytic effects when shale is thermally decomposed to produce oxides.

With these restrictions, the following rate expression is believed to be indicative of intrinsic oxidation kinetics for Anvil Points oil shale

$$r_c = kP^*_{O_2} \; C^o_c \; (1 - x) \quad (42)$$

where C^o_c is the initial char concentration, X is the fraction char converted, and $P^*_{O_2}$ is the oxygen partial pressure at the surface, specifically

$$kC_c^o = 8.47 \times 10^6 \exp\left[\frac{-23.2}{RT}\right] \qquad (43)$$

where kC_c^o has the units of $(atm\text{-}min)^{-1}$, T is in K, P_{O_2} is in atm and R is in $Kcal/mole^{-k}$.

O_2 Mass Transport

The fact that the kinetic experiments at temperatures greater than 550 C were under the partial influence of gas-solid mass transport has already been mentioned. Another consistent trend in the data was the failure of the high temperature, high conversion data to follow the apparent first order plot (see Figures 9 and 10). As will now be shown, this too can be explained in terms of gas-solid mass transport limitations.

First of all, if "quasi-steady state" can be assumed there is a steady state equivalency of mass transport and chemical reaction rates; i.e.,

$$k_g (P_{O_2} - P^*_{O_2}) = k C_c P^*_{O_2} \qquad (44)$$

where k_g is the gas-solid mass transport coefficient, k is the kinetic rate constant, C_c is the char concentration at any time, and P_{O_2} is the oxygen partial pressure in the bulk gas. If equation (44) is solved for $P^*_{O_2}$ in terms of the bulk gas oxygen pressure, P_{O_2}, and then substituted into equation (42), we obtain the following global rate expression

$$r_c = \frac{k C_c}{\left[1 - \frac{k}{k_g} C_c\right]} P_{O_2} \qquad (45)$$

At a constant oxygen partial pressure and temperature we can explain the high temperature data in Figures 9 and 10 by referring to the bracketed term in equation (45). At high temperature, the reaction rate constant, k, will be large and, at an early state of the reaction, C_c will be large. In this case $\frac{kC_c}{k_g} >> 1$ and the reaction rate becomes independent of char concentration, i.e., zero order. However as the reaction proceeds, the char concentration decreases until we have $\frac{kC_c}{k_g} << 1$ and the reaction rate becomes first order with respect to char concentration. Thus it is seen that high mass transport resistance can cause an apparent shifting order which is what is observed in the high temperature data of Figures 9 and 10. Further consideration of typical mass transport coefficients for these conditions indicated that equation (43)

is representative of the chemical kinetics at least up to the point at which carbonate decomposition occurs.

While equations (42) and (43) provide fundamental kinetic information and give an indication of the maximum oxidation rates to be expected from undecomposed shale, commercial retort operations will of course employ much larger shale particle sizes. In such cases, O_2 mass transport can be expected to play a more important role and provides the motivation for conducting experiments with the larger, cylindrical core samples described earlier. All of the experiments during this phase of the investigation utilized shale assayed at 17 GPT so that structural integrity remained intact after retorting. The continuous sample weight data provided measurements of fraction char converted as a function of time which were then compared to the analytical expressions developed by Levenspiel[40] in order to extract values of both the gas-solid convective mass transport coefficient, k_g, and the effective diffusivity of O_2 through the decharred portion of the sample, D.

Measurements of the effective diffusivity with samples oriented so that the diffusion path was radial, gave results which were consistently about three times lower than those measured with axial diffusion paths. It was concluded that the coring technique resulted in the creation of a thin, lower permeability layer near the cylindrical surface which produced artificially low diffusivities. Effective diffusivities measured with axial diffusion paths are considered to be more representative and were found to be independent of both oxygen concentration and temperature (425-525 C). These measurements gave diffusivity values of 30×10^{-6} m^2/sec for diffusion parallel to the bedding plane and 12×10^{-6} m^2/sec for diffusion perpendicular to the bedding plane. These measurements are consistent with those of Mallon and Braun[22] and the fact that diffusion perpendicular to the bedding plane is more difficult, is in agreement with Dockter's[1] results.

Convective mass transport coefficients were measured with the flow normal to the cylinder over a velocity range of 0.5 to 4.0 cm/sec. Figure 13 shows the results compared to the correlation of Ranz[41]. Note that the dependence on velocity is similar (square root) but that the data are lower than the correlation by a factor of about 2.5. This is typical of data collected at low partical Reynolds numbers (2-16 here) as pointed out by Kunii and Levenspiel[42].

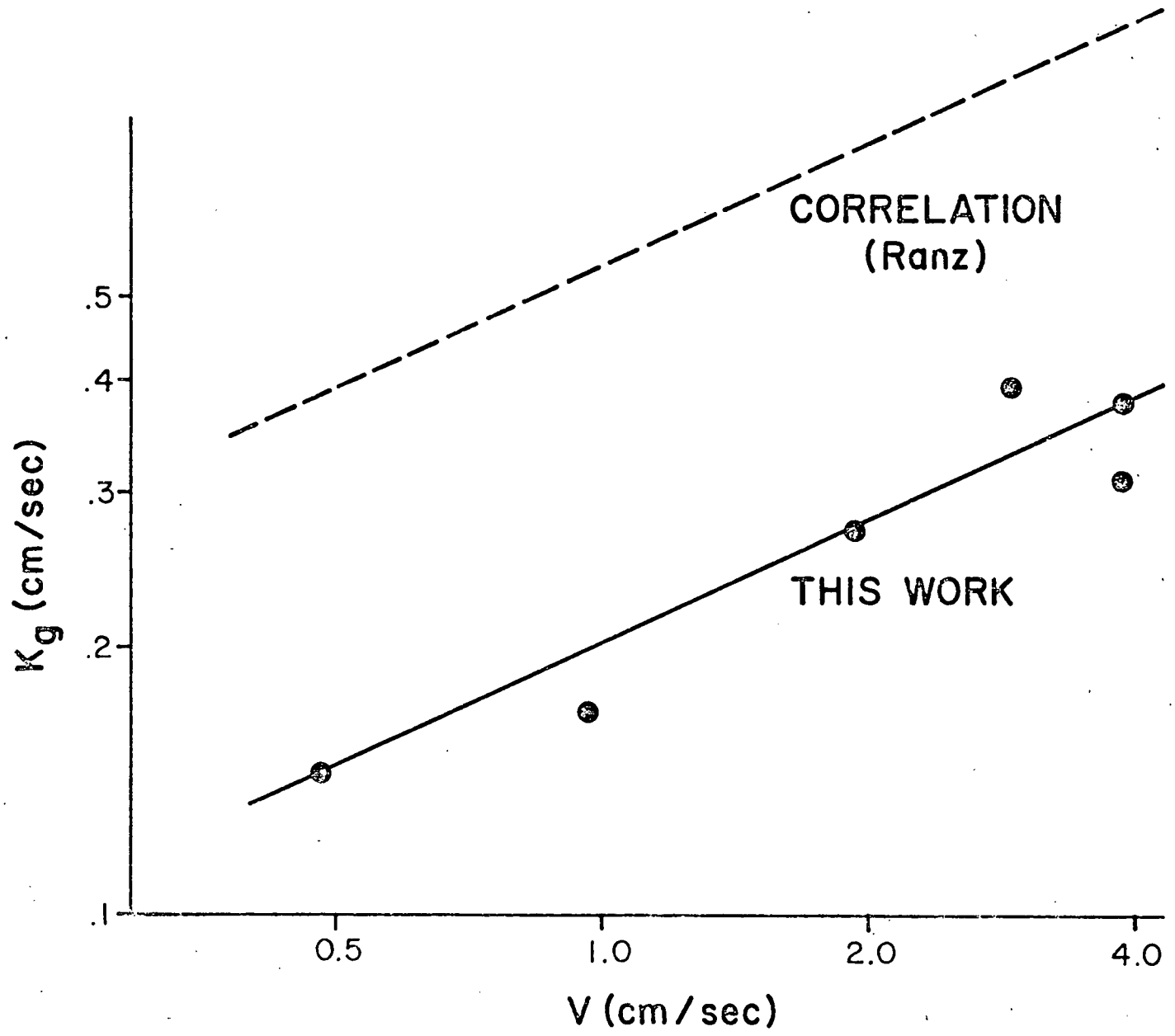

FIGURE 13: MASS TRANSFER COEFFICIENTS FOR CYLINDRICAL SHALE SAMPLE

Based on these measurements, calculations were then made to estimate the percentage of the total char oxidation resistance contributed by each of the three rate processes: oxidation kinetics, external mass transport (EMT), and diffusion. The calculations followed the equations given by Levenspiel[40] which predict the relative resistances as a function of conversion. Although the mass transport coefficients measured in this investigation would not be expected to directly apply to a fixed bed process such as in-situ retorting, there are a number of compensating factors. For example, mass transport coefficients are generally higher for single particles than the fixed beds but the actual interstitial velocities in fixed beds are higher than the superficial velocities. Also, there was no separate measurement here of the effect of particle size on kg. However, since we observed the same dependency on velocity as did Ranz[41], the calculations assume the same dependency on particle size, i.e, negative half-order.

Figure 14 shows these results for two different particle sizes (assuming spherical geometry) at a gas velocity of 2 cm/sec and at a temperature of 325 C. This temperature is in the neighborhood of the char ignition temperature and the velocity and particle sizes are not inconsistent with what might be encountered during in-situ retorting. At higher temperatures the resistance due to kinetics drops off rapidly and since the remaining two resistances are relatively independent of temperature, the values in Figure 14 can also be used to evaluate relative resistances at other temperatures. The interesting feature of these results is the importance of external mass transport. Even for large particles it contributes most of the resistance until 40% of the char has been oxidized.

Mineral Decomposition

The subject of mineral decomposition has been extensively studied at Lawrence Livermore Laboratories[11,15,16] and has been reviewed earlier in this report along with other pertinent investigations[12-14]. However, when it became apparent that recarbonation of CaO took place at a very high rate during char oxidation, it was decided to obtain separate kinetic data on the recarbonation of CaO.

At this point it is well to review the situation with respect to dolomite and calcite decomposition as shown below in Figure 15. In this scheme dolomite decomposition is shown as being able to decompose by two routes. In

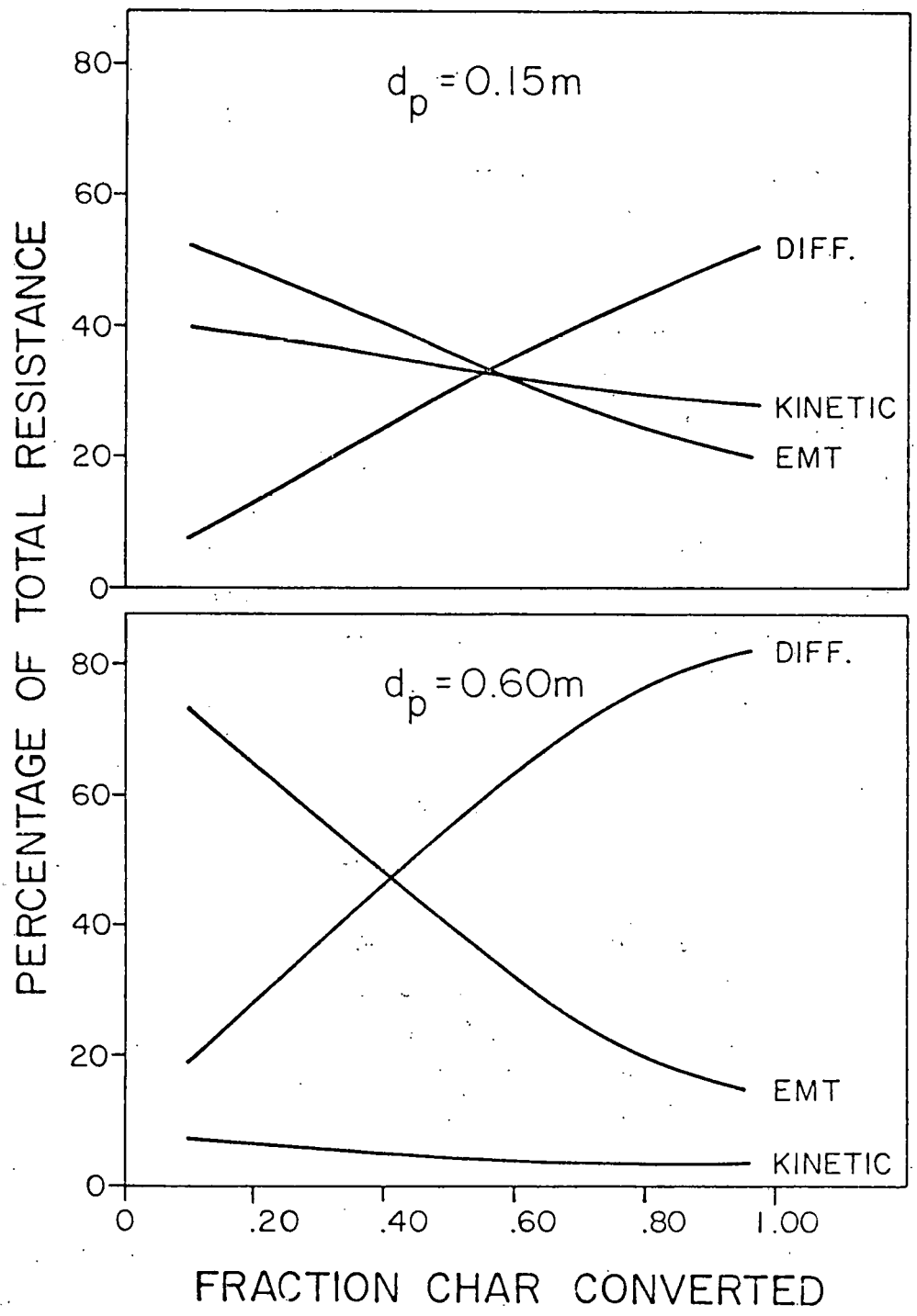

FIGURE 14: RELATIVE RESISTANCES FOR THE OXIDATION OF LARGE SHALE PIECES (325 C, 2 cm/sec)

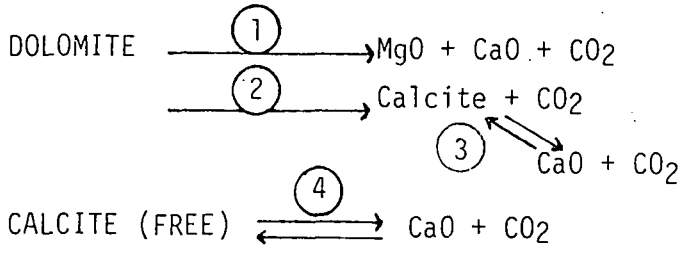

FIGURE 15
DOLOMITE/CALCITE DECOMPOSITION ROUTES

route (1) it decomposes directly to MgO and CaO and although this step is shown as being irreversible, there is no evidence to support such a one-step process. Route (2) has the dolomite first forming calcite which can then reversibly decompose to CaO by route (3). In addition to dolomite, "free" calcite is also present in Anvil Points oil shale and it too can decompose reversibly to CaO. Because of the reversible nature of calcite decomposition it can be inhibited and, in fact prevented, by having sufficiently high CO_2 pressures (depending on the temperature).

The work carried out at Lawrence Livermore Laboratory[15] concentrated only on the decomposition of the oil shale minerals although the inhibitory effect of P_{CO_2} on calcite decomposition was accounted for, as shown in equation (5).

$$d(MCO_3)/dt = k_f(MCO_3)\,[1 - P_{CO_2}/Keq] \qquad (5)$$

In their work no distinction could be made between dolomite and calcite decomposition. Thus, equation (5) was used for both with the exception that the inhibiting effect of P_{CO_2} was removed in the case of dolomite decomposition. In the work reported here the samples were initially decharred and decarbonated in helium so that CaO would be formed ($P_{CO_2} \sim 0.005$ atm). Recarbonation kinetics were obtained by passing sweep gases containing various CO_2 partial pressures over the decarbonated samples at temperatures ranging from 425 C to 725 C. The rate of recarbonation was determined from the continuous gravimetric measurements. After each sample was recarbonated, the sample was decarbonated a second time to get kinetic data on the decarbonation rates. The following rate expression was developed from this study:

$$d(CaCO_3)/dt = k_f\,(CaO)\quad\left(1 - \frac{P_{CO_2}(CaO)}{Keq(CaCO_3)}\right) \qquad (46)$$

Where k_f is the decomposition rate constant:

$$k_f = 1.05(10)^8 \exp(-40.9/RT) \quad (47)$$

and the equilibrium constant, Keq is given by

$$Keq = 6.19(10)^7 \exp[-41.7/RT] \quad (48)$$

The rate expression assumes that the activities of the two solid phases are 1.0, and that the surface areas of the calcite and CaO are proportional to the amount of each mineral present.

In comparing the results given by equation (46) with Campbell's[15] results given in equation (5), the difference is seen to lie in the assumptions made concerning the surface areas of calcite and CaO. Campbell assumed that the surface area of calcite was the same as the CaO surface area. However equation (46) was derived by assuming that the surface areas of the two were proportional to the quantity of each present at any time. Table 4 compares the predictions of these two expressions as a fraction of calcite converted at two temperatures for P_{CO_2} = 0.01 atm.

TABLE 4

COMPARISON OF CALCITE DECOMPOSITION RATES

(P_{CO_2} = .01 atm)

dx/dt (min^{-1})

	675 C		750 C	
x	Eq (5)	Eq (46)	Eq (5)	Eq (46)
0	0.0043	0.047	0.373	0.189
.2	0.0034	0.026	0.300	0.146
.7	0.0013	0.008	0.112	0.040

As can be seen, the results are quite different, particularly at the lower temperature where equation (5) predicts a decomposition rate which is a factor of ten lower than that predicted by equation (46). At the higher temperature, equation (5) predicts a higher rate by a factor of about 2. The difference in the predictions at 750 C is due to the higher activation energy reported by Campbell but the difference at the lower temperature is due to the much larger inhibitory effect of P_{CO_2} in his expression. For example, the initial calcite decomposition rate (x = 0) is inhibited by 90% in equation (5) whereas, since there is no CaO present under these conditions, there is no initial CO_2 inhibition predicted by equation (46). Since equation (46)

was derived on the basis of recarbonation as well as decarbonation, it would seem that this should be more representative of the reversible reaction rate.

Recall that the results obtained during char oxidation with thermally decomposed char indicated that the recarbonation might very well proceed via a surface active step.

$$CO_2 + CaO \rightleftarrows CaO \cdot CO_2 \qquad (49)$$

$$CaO \cdot CO_2 \rightleftarrows CaCO_3 \qquad (50)$$

Since the recarbonation rate was found to be significantly higher when CO_2 was supplied by char oxidation, it was proposed that CO_2 was already adsorbed in that case. This would further indicate that not only does recarbonation follow a two step reaction sequence, but that the first step, equation (40), is the slowest step. In other words, when CO_2 is supplied by the bulk sweep gas, we are in essence measuring the kinetics of equation (49), but when it is already on the surface (as in char oxidation), we measure the kinetics of equation (50). This could easily explain the discrepancies in Table 4 and points to the need for more fundamental work along these lines.

CO_2 Gasification

The only reported study of the CO_2 gasification of oil shale char is the work of Burnham[16,23,24] at Lawrence Livermore Laboratories. His results have already been discussed in detail (see equations [24]-[26]) and were largely empirical in nature. Becuase of the large uncertainty in the reaction order with respect to CO_2 (0.2 ± 0.2)[23] it was decided to attempt a separate determination of the reaction order, using the nonisothermal technique described earlier.

Using a heating rate of 2°C/min, and CO_2 partial pressures between 0.016 and 1 atm, the CO_2 gasification rate was determined by gas chromatographic measurements of the CO production detected in the exit gases. The char present at any time was found by numerical integration of the

rate of CO production. Burnham's results indicated that CO_2 gasification was first order with respect to char and this was also found to be the case here. Initial attempts to determine the reaction order with respect to CO_2 indicated that the apparent reaction order decreased with increasing P_{CO_2}. Consequently the following rate expression was proposed:

$$r_c/C = \frac{k_1 P_{CO_2}}{1 + K_2 P_{CO_2}} \tag{51}$$

The reciprocal of equation (51) can be rearranged to a linear equation:

$$C/r_c = K_2/k_1 + 1/k_1 \ (1/P_{CO_2}) \tag{52}$$

so that a straight line results with a slope of $1/k_1$ and an intercept of k_2/k_1. The data, plotted according to equation (52), are shown in Figure 16 at three different temperatures. The constant k_1 was found to vary with temperature and the Arrhenius plot shown in Figure 17 was used to develop the following expression for k_1:

$$k_1 = 4.68(10)^8 \exp(-44.3/RT) \tag{53}$$

where the units for k_1 are $min^{-1}\ atm^{-1}$. The constant k_2 was found to be independent of temperature and the average value for these experiments was:

$$K_2 = 4.95\ atm^{-1} \tag{54}$$

It is interesting to compare this rate expression to equation (20) for the CO_2 gasification of coke. Both expressions have about the same activation energy for the rate constant k_1. Also the adsorption constant K_3 in equation (20) varies from about 5.6-4.7 over the same temperature range. The reactivity of the coke however is about 300 times less than the char present in the shale.

It is also interesting to compare the CO_2 gasification rates obtained here with those measured by Burnham[23]. As can be seen from Table 5, Burnham's rates are about three times higher than those measured here. At this point there is no obvious reason for the difference in char reactivity although

FIGURE 16

Determination of rate constants k_1 and k_2 for Equation (51) at various temperatures

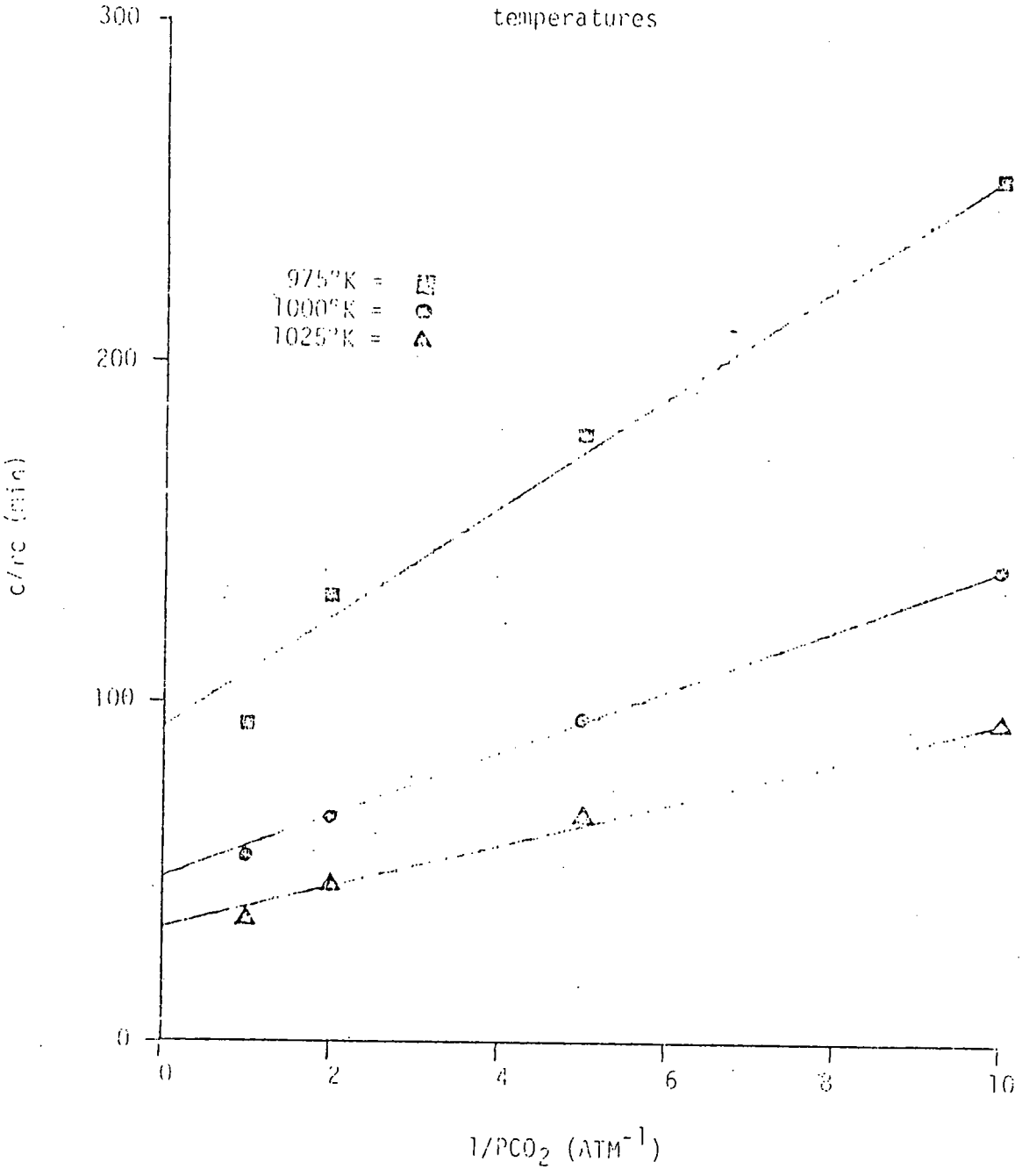

FIGURE 17

Arrhenius plot for values of k_1

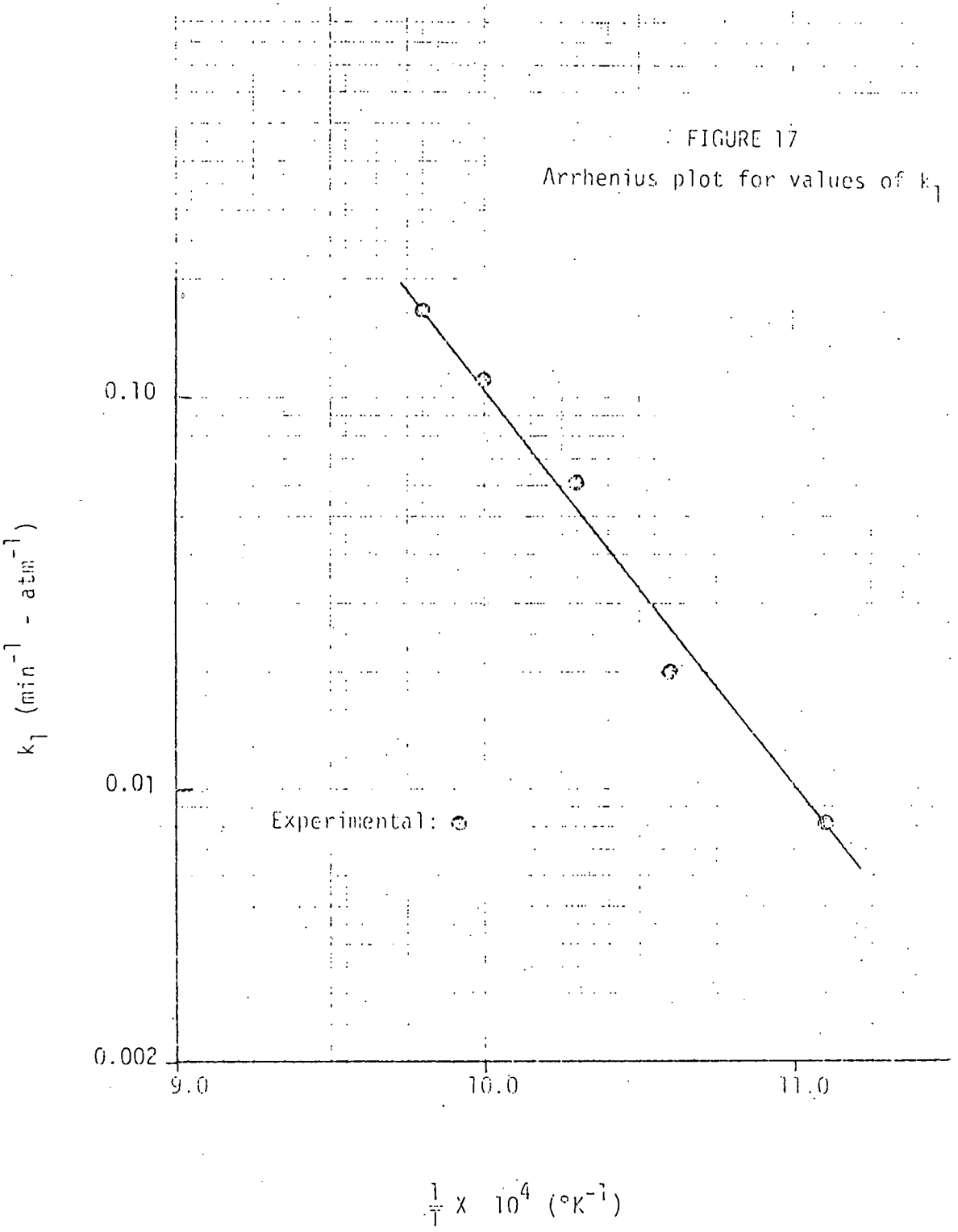

Burnham did note that both HCl leaching and thermal pretreatment reduced the reactivity substantially. However the samples used here were apparently

TABLE 5
COMPARISONS OF CO_2 GASIFICATION RATE
(T = 700C)
$r_c/C \times 10^2$(Min)

P_{CO_2} (Atm)	LLL Rate[23]	This Work
0.1	1.8	0.35
0.3	2.2	0.63
0.7	2.6	0.82
1.0	2.8	0.88

treated in the same manner described by Burnham. It is possible that the answer lies in some of the other reactions which take place in a non-isothermal experiment. At the CO_2 partial pressures used in both experiments calcite would not be expected to decompose to CaO but it would react to form silicates at temperatures above 700C. When this occurs, CO_2 is liberated at the surface and, as will be shown later, is very reactive. It is possible that the difference in the assays of the shale used in the two sets of experiments (Burnham used 22 GPT shale, 50 GPT shale was used here), is the reason for the discrepancy. That is, the higher concentration of minerals in the lower assay shale could have produced more surface CO_2 which then resulted in a higher gasification rate. Again this is a subject deserving of more study.

The fact that the presence of CO on the surface may have a significant inhibiting effect on the overall gasification rate has already been mentioned. One experiment was performed to assess the significance of the presence of CO in the sweep gas. The inhibitive effect of CO was determined by observing the sample weight loss rate for various partial pressures of CO at a constant temperature of about 1000°K and a fixed CO_2 partial pressure of .5 atm. The maximum ratio of partial pressure of CO to CO_2 in the inlet gas was set so that equilibrium $[(P_{CO}/P_{CO_2})_{eq} = 1.0]$ was not approached for this reaction $(P_{CO}/P_{CO_2})_{max} = .6)$. In this experiment,

an unexplained weight increase was initially observed when 0.3 atm of CO was first passed over the sample (this will be discussed in more detail below). After the weight stablized, the experiment was continued and the char consumption rates measured in this experiment for various CO partial pressures is tabulated in Table 6.

TABLE 6

EFFECT OF CO ON CO_2 GASIFICATION OF CHAR

(P_{CO_2} = .5 atm, Temp. = 1003°K)

P_{CO} (atm)	r_c/C (1/min)
.3	0
.1	.0029
.05	.0035
.00	.0074

These rates are only approximate due to the small weight loss observed, but assuming that the weight losses observed were due solely to the gasification of char, it was apparent that the presence of CO at partial pressures as low as .05 atm had a significant inhibiting effect on CO_2 gasification rate. Using the results in Table 6 and solving the rate expression:

$$r_c/C = \frac{k_1 P_{CO_2}}{1 + K_2 P_{CO_2} + K_3 P_{CO}} \qquad (55)$$

for k_3 gave values of 32 and 48 using CO partial pressures of .1 and .05 atm respectively. These values also compare very well with the values given for coke in equation (20), at this same temperature. It is therefore obvious that CO inhibition is significant and more research is necessary to obtain k_3 as a function of temperature and to also explore the possible inhibition effects of other species which could be present in in-situ applications (H_2 for example).

Steam Gasification

Kinetics. Once again the only reported measurements of the rates of the steam-oil shale char reaction are those of Burnham[36]. In that study the non-isothermal kinetic data were analyzed empirically and, as in the case of the CO_2-char reaction, two parallel rate expressions were used to fit the data (equations [30]-[32]). Although Burnham reported that the steam gasification rate appeared to be one-half order with respect to steam, his final rate expression did not have a steam pressure dependency and appeared to apply only to P_{H_2O} = 1 atm.

Because of the empirical nature of Burnham's results, an attempt was made here to obtain and interpret steam gasification in a more fundamental manner. There are actually at least three basic reactions which take place during steam gasification.

$$C + H_2O \rightarrow CO + H_2 \quad (27)$$

$$CO + H_2O \rightleftarrows CO_2 + H_2 \quad (28)$$

$$CO_2 + C \rightarrow 2CO \quad (17)$$

The second reaction (equation [28]), the water gas shift reaction, is known to occur to a great extent over oil shale[2,36] and can result in a make-gas almost totally devoid of CO_2. Once appreciable quantities of CO_2 are produced, CO_2 gasification (equation [17]) can also occur. Any fundamental analysis of steam gasification data must account for all three reactions.

The kinetic studies discussed here were all based on data collected in the presence of shale which had been thermally decarbonated to the oxides. Again, the decarbonation was conducted at 675C in the presence of helium. At this temperature a loss of char (due to CO_2 gasification) on the order of 5-10% was experienced.

The first attempt at data analysis was a simple power law expression to represent the rate of char consumption. For isothermal experiments (760-870C) at constant values of P_{H_2O} (.13-.75 atm), a first order plot in terms of the fraction char converted was found to give consistent

straight lines under all conditions. This indicated that steam gasification was first order with respect to char. The slopes of these lines were then plotted on log-log paper as a function of P_{H_2O} in order to determine the reaction order with respect to steam. If the reaction order is constant, straight lines of the same slope should result at each temperature. Figure 18 shows a definite deviation from a straight line, with the apparent reaction order varying from one-half order at low steam pressures to approximately first order at high pressures.

Some insight into the mechanisms at work can be obtained from the G.C. analyses of the exit gases which are shown as a function of time for a typical run in Figure 19. Note that the CO make is minimal and the H_2/CO_2 ratio is on the order of 2. In view of the stoichiometry of equations (27), (28), and (17), it is obvious that the water gas shift reaction is playing a major role in the reaction sequence. The data were then tested to determine whether the water gas shift reaction was at or near chemical equilibrium. The equilibrium constant for this reaction is defined as:

$$Keq = \frac{P_{CO_2} P_{H_2}}{P_{CO} P_{H_2O}} \qquad (56)$$

The partial pressure ratio as defined by the right hand side of equation (56) is plotted as a function of time for a run at 815C in Figure 20. At this temperature the equilibrium constant is equal to 0.98 and, as can be seen, the partial pressure ratio increases, approaches Keq at about 6 minutes, and then decreases. This can be explained by an early predominance of equation (27) to build up concentrations of CO. At this point the rate of the water gas shift reaction increases which serves to increase the CO_2/CO ratio and the H_2 make. Finally, the increased concentration of CO_2 accelerates the CO_2 gasification rate causing the partial pressure ratio in equation (56) to drop significantly.

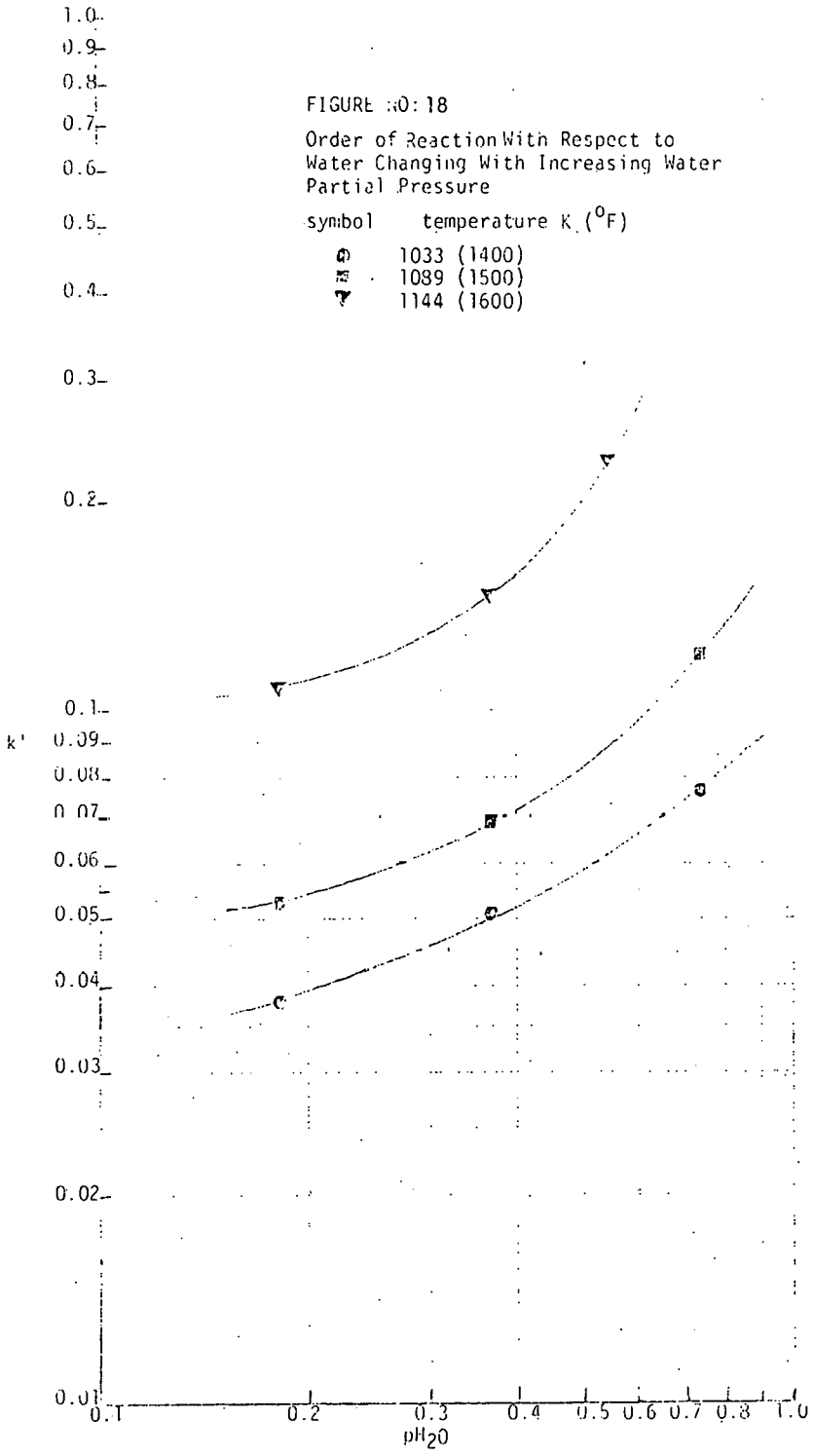

FIGURE 30:18

Order of Reaction With Respect to Water Changing With Increasing Water Partial Pressure

symbol	temperature K (°F)
○	1033 (1400)
□	1089 (1500)
▽	1144 (1600)

FIGURE NO: 19

Make Gas Composition at 1089 K (1500°F) and pH_2O equal to 0.184

symbol	gas
⊕	H_2
⊡	CO_2
○	CO

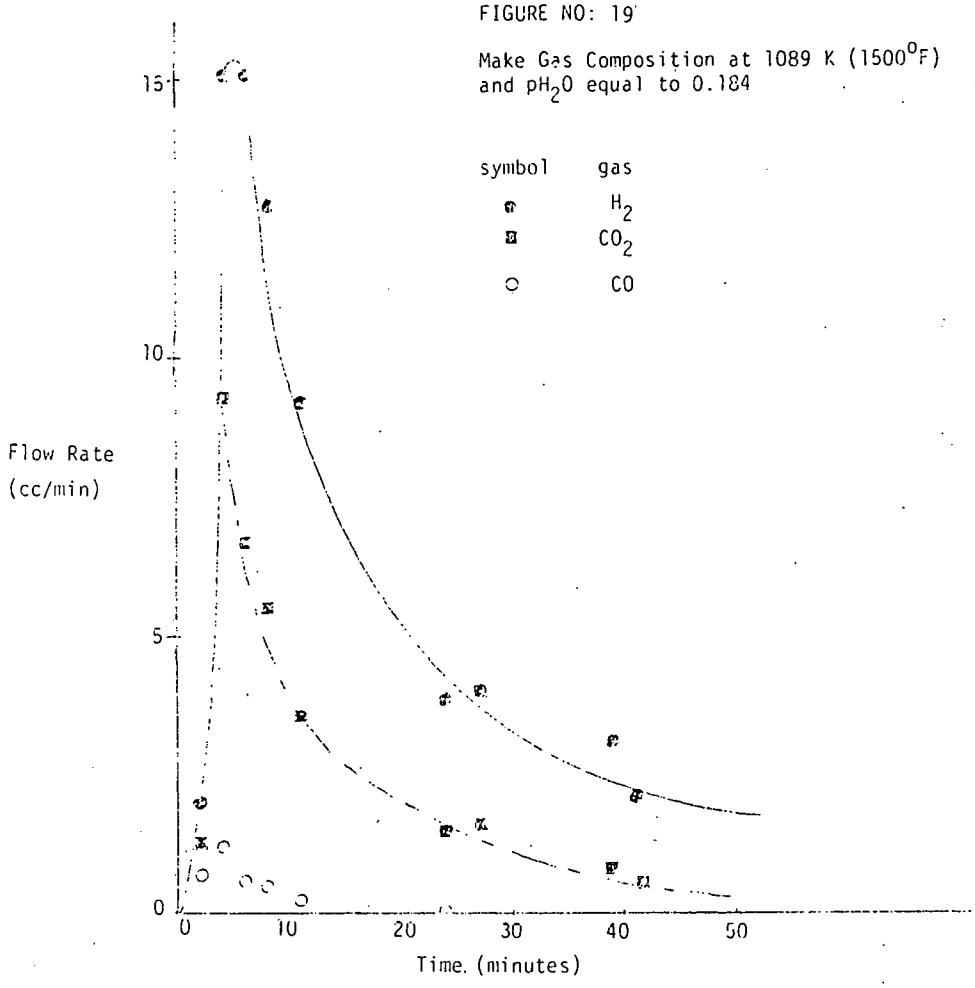

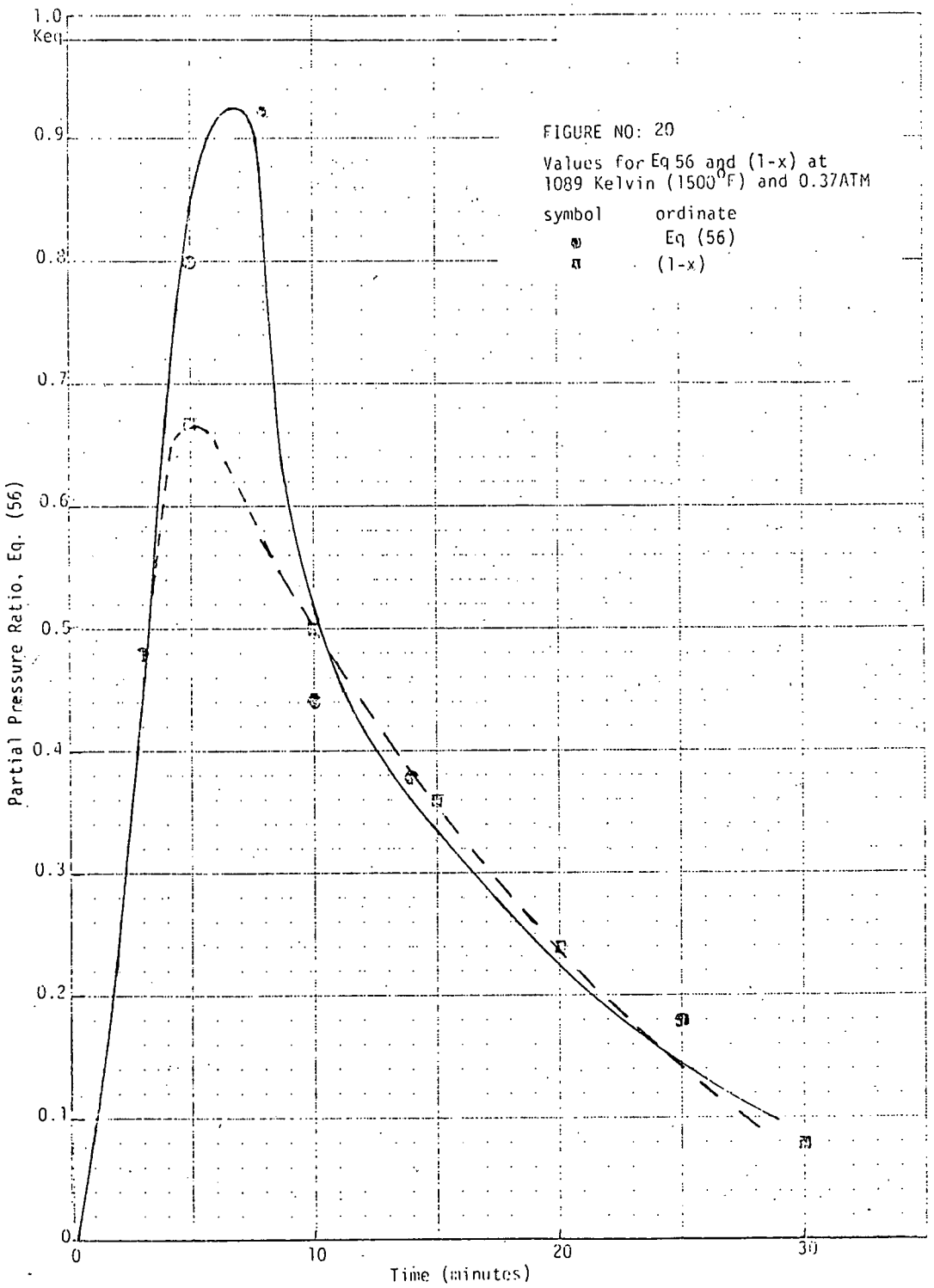
1.0
Keq
0.9
0.8
0.7
0.6
0.5
0.4
0.3
0.2
0.1
0
Partial Pressure Ratio, Eq. (56)
0
10
20
30
Time (minutes)
FIGURE NO: 20
Values for Eq 56 and (1-x) at
1089 Kelvin (1500°F) and 0.37ATM
symbol ordinate
Eq (56)
(1-x)

With these observations it was decided to attempt to match the observed kinetic data with a dynamic simulation of the rates of the three pertinent equations. The kinetic expression for CO_2 gasification has already been derived (equation [51]) and thus it remained to develop kinetic expressions for equations (27) and (28). In the absence of a separate and detailed kinetic study of the water gas shift reaction, a simple elementary reaction rate expression was proposed

$$r_s = k_s \left(P_{CO}\, P_{H_2O} - \frac{1}{Keq_s}\, P_{H_2}\, P_{CO_2}\right) \qquad (57)$$

Since there is no separate evidence for the form of equation (57), this is strictly conjecture at this point. However, its advantage is that it not only accounts for the inhibiting effects of CO_2 and H_2 but it will also produce a zero rate if chemical equilibrium is reached. On this basis then, the only unknown is the forward rate constant, k_s.

The problem of the rate of steam gasification is made tractable by the realization that at time = 0, the only reaction occurring is equation (27). Thus, by examining the initial rates, the reaction order with respect to steam was found to be one-half order and the activation energy of the C + H_2O reaction was equal to 20.6 Kcal/mole. Turning now to the reaction order with respect to char, note that only equations (27) and (17) consume char, and the rate of the latter reaction has already been determined to be first order with respect to char. If equation (27) is also first order and if P_{CO_2} can be assumed to be constant, then a plot of ln(1-x) vs. time should produce a straight line. Such a plot is shown in Figure 21 and reasonable straight lines do result. The slight S-shaped pattern of the actual data points about the line is attributed to the fact that P_{CO_2} is not strictly constant. In fact, for all three runs, P_{CO_2} dropped from .01 atm near the beginning of the run to .001 atm at the end. Although this is a change of a factor of ten, it should be noted that CO_2 gasification only accounts for about 3% of the char consumption at low temperatures (750C) and about 17% at the highest temperatures (860C).

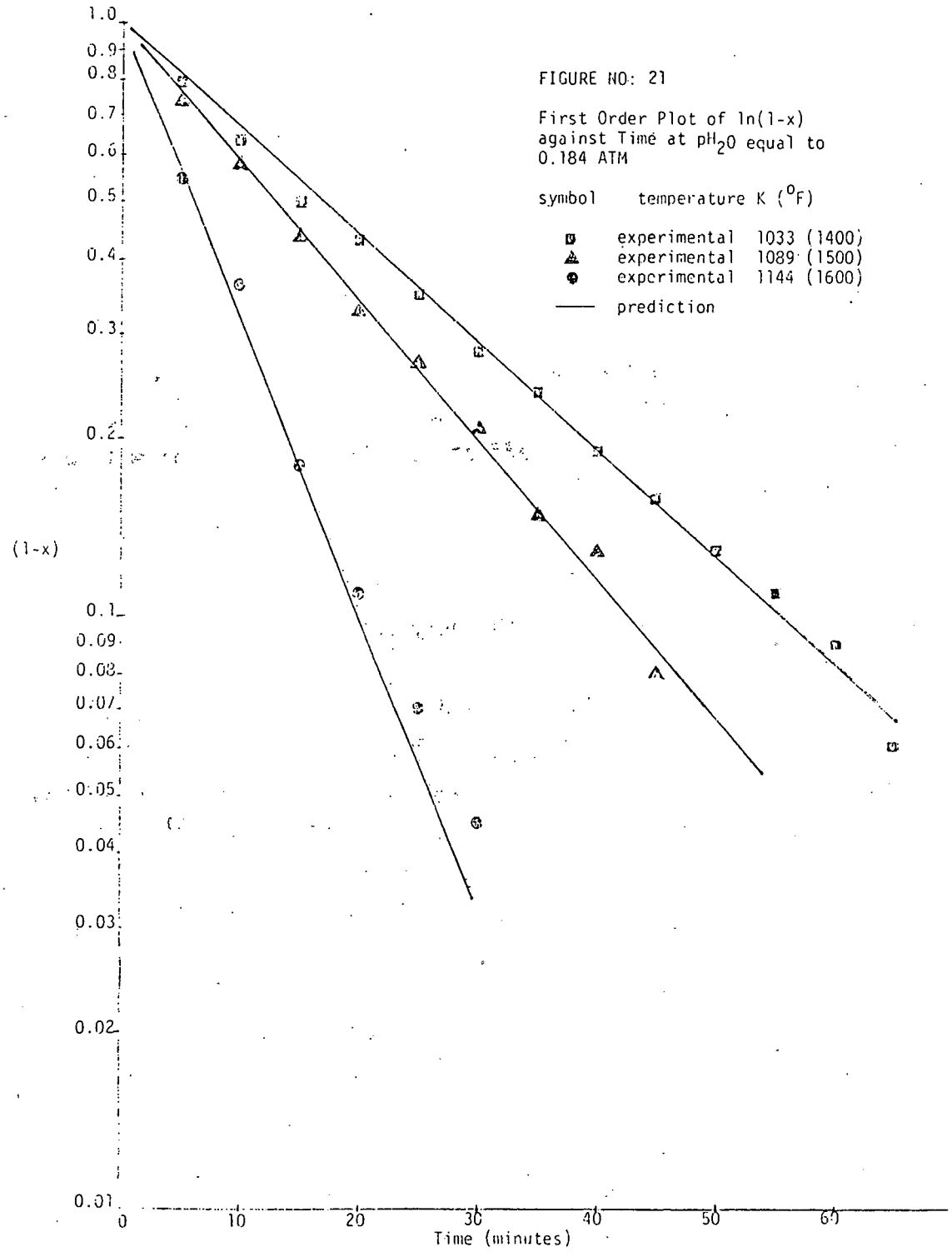

FIGURE NO: 21

First Order Plot of ln(1-x) against Time at pH_2O equal to 0.184 ATM

symbol		temperature K (^oF)
▫	experimental	1033 (1400)
△	experimental	1089 (1500)
⊕	experimental	1144 (1600)
——	prediction	

Thus an applicable kinetic expression for equation (27) is

$$r_{sg} = k_{sg} P_{H_2O}^{.5} C_c \tag{58}$$

where

$$k_{sg} = 2.1 \times 10^3 \exp\left[\frac{-20.6}{RT}\right] \tag{59}$$

In order to ascertain whether the set of three equations does indeed describe steam gasification, it is necessary to determine k_s and then see if the measured data can be predicted from a solution of the three equations. To do this, the differential equations describing the concentrations of CO, CO_2, and H_2 in the reactor were solved using the IBM CSMP computer program. Values of k_s were chosen until equilibrium of the water gas shift reaction was approached at about t = 5 min. A value of k_s = 10 atm^{-2} - min^{-1} appeared to achieve this for all runs and was then held constant for the remainder of the evaluation.

With these values, the dynamic simulation of steam gasification was able to predict the char consumption versus time curve to within 5% of the measured values. Additional insight into the validity of this simulation can also be obtained from Table 7 which shows a comparison of the predicted and measured product gas ratios.

TABLE 7

Comparison of Product Gas Ratios

TEMP (°F), pH_2O (atm)	TIME (min)	CO/CO_2 PRED.	CO/CO_2 EXP.	H_2/CO_2 PRED.	H_2/CO_2 EXP.
1400, 0.184	4	0.06	0.103	2.06	2.42
	24	0.03	0.08	2.03	2.84
	39	0.01	0.28	1.94	3.04
1400, 0.74	3	0.03	0.05	2.03	1.89
	7	0.02	0.034	2.02	1.81
	9	0.02	0.038	2.02	1.84
1600, 0.184	3	0.09	0.30	2.09	2.32
	9	0.05	0.11	2.05	2.97
	11	0.04	0.14	2.04	3.36

It is interesting that a reasonable match to the data is obtained except at higher char conversions and temperatures and low P_{H_2O}. Note also that, in these cases, the experimental H_2/CO_2 ratios are higher than predicted and the CO/CO_2 ratios are lower than predicted. This can be explained if the CO_2 gasification rate predicted by equation (51) is too low. Recall that the CO_2 gasification rates measured here were lower by a factor of about three than those reported by Brunham[23]. One explanation was that the CO_2 released by the mineral reactions which accompanied CO_2 gasification in Burnham's experiments, was surface active and caused an increased gasification rate. If this is the case, the same phenomena could be occurring here. Since the shale evidently catalyzes the water gas shift reaction, CO_2 would be produced on the active surface and would presumably be more accessible to further react with the char. Additional evidence of this will be given below during the discussion of kinetic interactions.

Table 8 shows a comparison of the steam gasification rates obtained from this work (equations [58] and [59]) with those given by Burnham[36] (equations [30] - [32]). As this table shows, Burnham's rates are anywhere from 3 to 7 times higher with the discrepancy being larger at the higher temperature. The latter is due to the very high activation energies

TABLE 8
COMPARISON OF STEAM GASIFICATION RATES

$(dx/dt)_o$ (min^{-1})

Temp →	750C		850C	
P_{H_2O} →	.18	.74	.18	.74
This Work	.035	.072	.087	.177
Burnham[36]	.095	.193	.641	1.30

reported by Burnham. There is no apparent explanation for this discrepancy other than the fact that Burnham based his rate expression solely on the H_2 production rate. As shown above, steam gasification is at least as complex as the three reactions used in this analysis. Lumping

all effects into one empirical rate expression can lead to predictive problems for conditions different than those upon which the expression is based. Another factor which should not be overlooked is the possibility that the char used in Burnham's studies was more active than that used here. Although no effect of assay was observed in the case of char oxidation, this was not examined for either CO_2 or steam gasification. Since Burnham used 22 GPT shale and 50 GPT shale was used here, this remains a distinct possibility and should be examined further.

Catalytic Effects. A thorough discussion of mineral catalysis has already been given for char oxidation. These effects were also examined for steam gasification and a comparison of the gasification of unleached and acid leached shale is given in Figure 22. Note that while, in the case of char oxidation there was no effect of acid leaching, the same is not true here. In fact the results here are very similar to those reported by Burnham[23] for CO_2 gasification where HCl leached shale had only about 10% of the activity of unleached shale. This points to the possibility of a different catalytic effect in the case of char gasification. It was not possible to obtain unambiguous steam gasification rate data in the presence of undecomposed calcite because of the high temperatures required for gasification. At these temperatures calcite will rapidly decompose to CaO unless there is a high enough CO_2 pressure to prevent it. At these temperatures, P_{CO_2} values in excess of 0.10 atmospheres are required and the rate of CO_2 gasification becomes signficant. This will be covered in the discussion of kinetic interactions.

Iron was ruled out as a catalyst for char oxidation because HCl leached shale (which removes iron) had the same oxidation rate as unleached shale. However it is highly possible that iron is the operative catalyst for char gasification. In separate experiments, decharred shale was exposed to CO and H_2 at a temperature of 750C and a noticeable mass loss of about 50 mg was experienced. It was concluded that iron was being reduced to a lower oxidation state and this was partially verified by the fact that a 50 mg weight gain was experienced when the "reduced" sample was

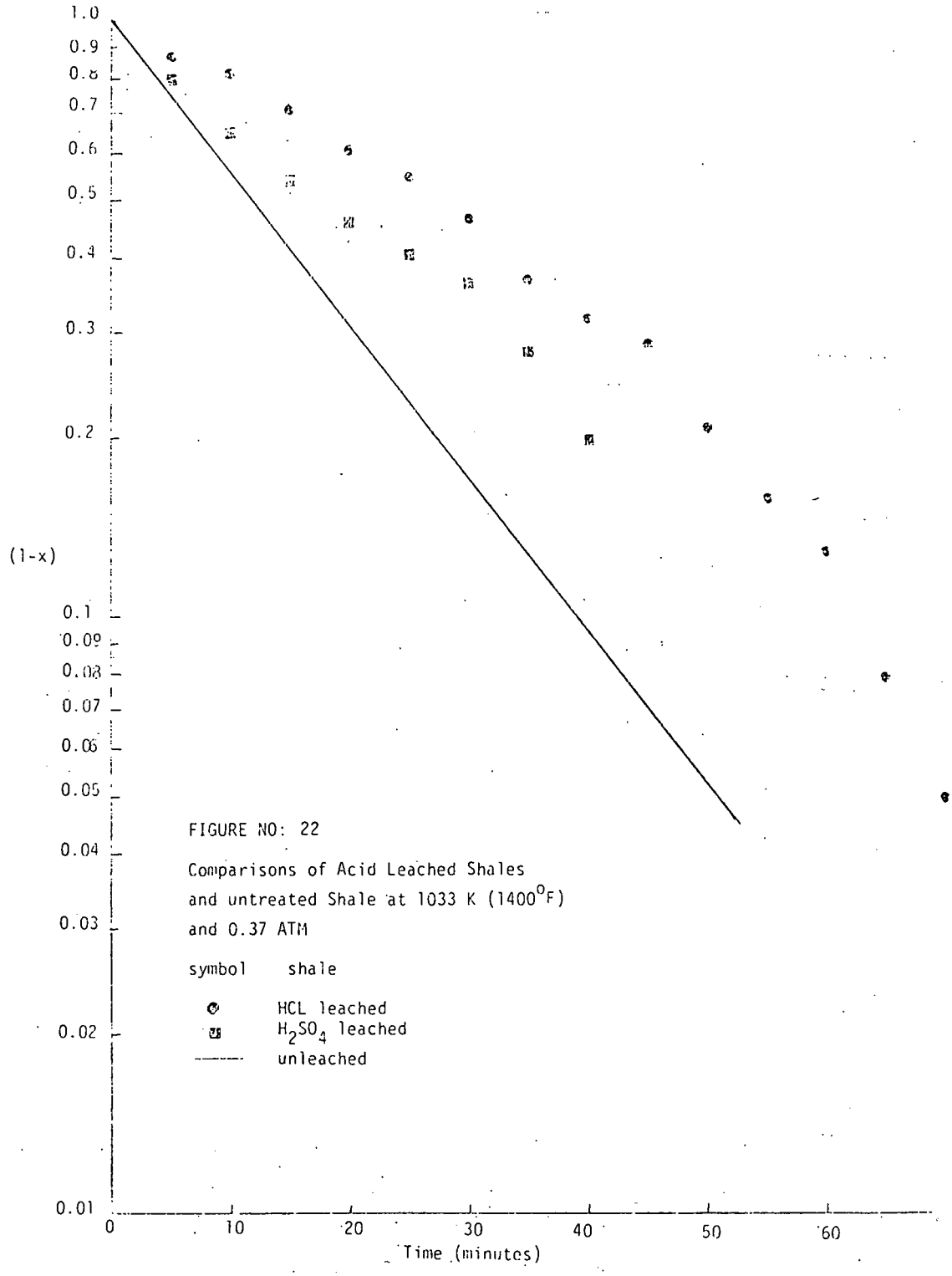

FIGURE NO: 22

Comparisons of Acid Leached Shales and untreated Shale at 1033 K (1400^{O}F) and 0.37 ATM

symbol	shale
⊙	HCL leached
⊡	H_2SO_4 leached
———	unleached

exposed to air. This phenomenon appeared to be totally reversible and H_2 reduction was faster and more complete than CO reduction. Oxidation, on the other hand, could also be partially effected using CO_2 although the rate was much slower. It should be pointed out that similar observations have been made by Campbell[43] in studies of CO oxidation over spent shale samples. Obviously these observations have significant implications since CO, CO_2 and H_2 are all present during steam gasification. Additional studies of the oxidation/reduction of iron are necessary before a complete understanding of char gasification can be obtained.

Kinetic Interactions

Up to this point all of the kinetic data correspond to single reactions although other reactions were found to play a role during steam gasification. Work conducted at Lawrence Livermore Laboratories (LLL)[15,16] however, did consider the effects of steam and CO_2 on mineral decomposition and their empirical rate expressions were discussed in the BACKGROUND section. The possibility exists that reactant mixtures, as would be present in a commercial retorting situation, could result in alterations of selectivity which would not be predicted by the combination of rate expressions derived both here and at LLL. This could be due, for example, to preferential adsorption steps since some of the results point to the existence of surface active species.

As a result, both non-isothermal and isothermal experiments were conducted using various reactant mixtures and the data were compared to the predictions of a dynamic model which was in turn based on the kinetic expressions derived here and at LLL. The mineral decomposition rate expressions used in the model were those given by LLL (equations (8) - (16)). Even though the rate data obtained here for dolomite/calcite decomposition in the presence of helium were found to be lower than that observed by LLL (Table 4), only LLL has accounted for the effect of steam on mineral decomposition. Also, at the time the kinetic interaction study was conducted, only LLL's steam gasification rate was available. Consequently the model utilized LLL's reaction expressions for those reactions and the CO_2 gasification rate expression derived in this work (equations (51), (53), and

(54)). It was assumed that the latter was more representative in view of the large uncertainty associated with the CO_2 reaction order derived at LLL (equations (24) - (26)).

Mineral Decomposition in CO_2 Environment. A series of non-isothermal experiments were conducted with CO_2 partial pressures varying from 0.1 to 1.0 atm. Since the maximum temperatures reached in these runs was about 800°C, three reactions are expected to take place: dolomite decomposition to calcite (equation (2)), the formation of silicates (equation (4)) and the CO_2 gasification of char. Comparisons of the measured experimental sample weights with that predicted by the model are shown in Figures 23 and 24 for CO_2 partial pressures of 1.0 and 0.2 atm. It should be pointed out that the heat-up rates given in these figures are only average values. At times the temperature programmer caused heat-up rates as high as 4 C/min. The computer calculations however, are based on the actual measured temperatures.

What is apparent from Figures 23 and 24 is that the model predicts higher decomposition rates than are measured, with the discrepancy being higher at the lower P_{CO_2}. Since the CO_2 gasification rate expression used here (equation (51)), predicts lower rates than LLL's expression, this cannot be the reason for the discrepancy. Evidently the CO_2 concentration has an effect on mineral decomposition which is not predicted by the model. Recall that LLL's results (equations (8) - (11)) predict an inhibition of silicate formation by the presence of CO_2 as long as P_{CO_2} is greater than the $CaCO_3$-CaO equilibrium constant. This was true in all of these runs except for the one experiment conducted at P_{CO_2} = .10 atm where this was not the case at temperatures above 700 C. Looking more closely at Figures 23 and 24, it can be seen that the *rate* of weight loss is close to that predicted by the model but that the model predicts more significant decomposition at the lower temperatures. Since only dolomite would be expected to decompose at these lower temperatures it is possible that it is the dolomite rate which is in error. This is partially substantiated by the results shown in Table 9 which gives the experimental and predicted sample weights at the point in the run where the predicted silicate formation has just reached 1 mg (CO_2 evolved).

FIGURE 23

Sample Weight for Experiment T-2

P_{CO_2} = 1.0 atm

Average heat up rate = 2.1°K/min

T = 756°K at time = 0

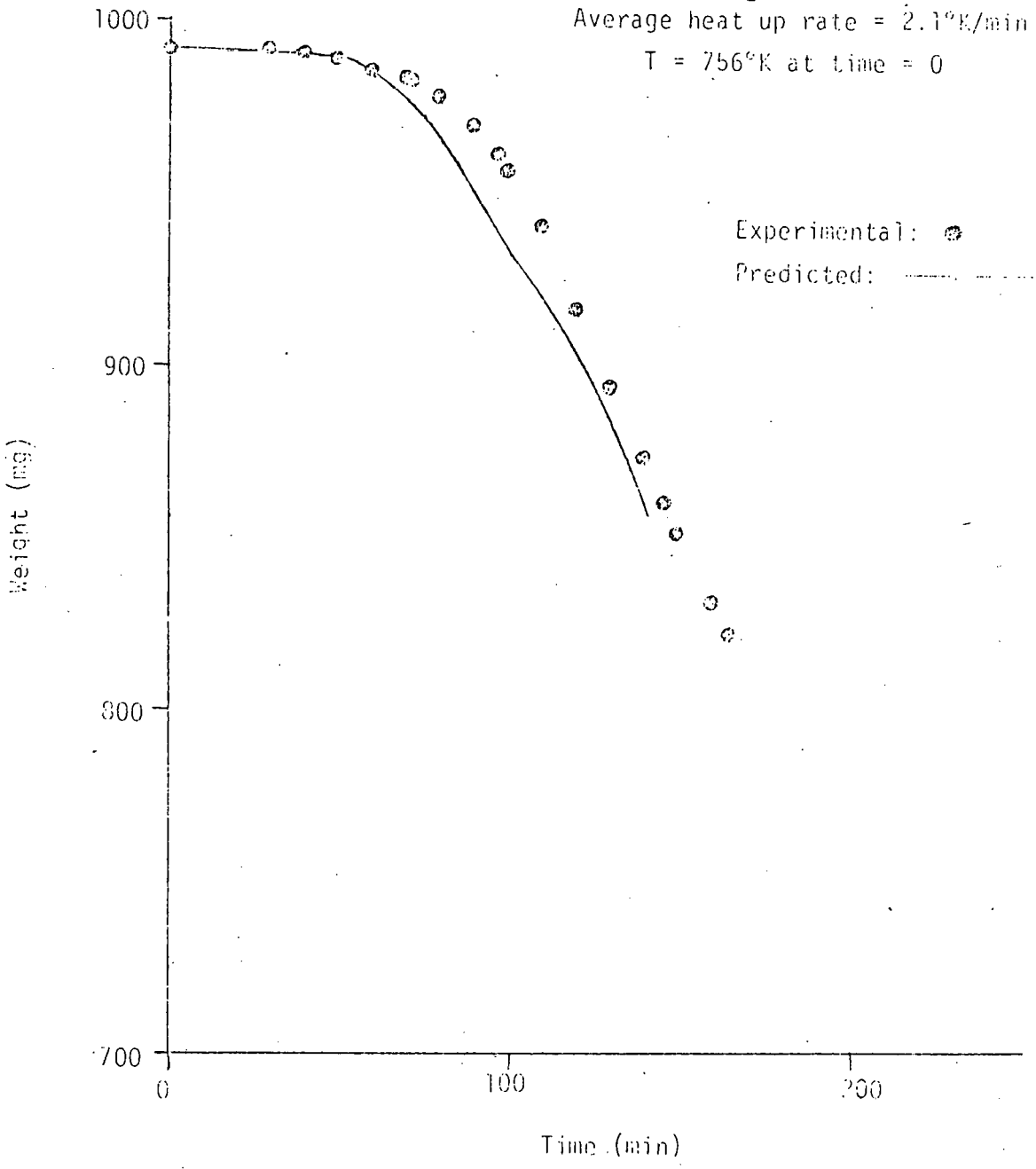

FIGURE 24

Sample Weight for Experiment T-17

P_{CO_2} = .2 atm

Average heat up rate = 2.0°K/min

T = 756°K at time = 0

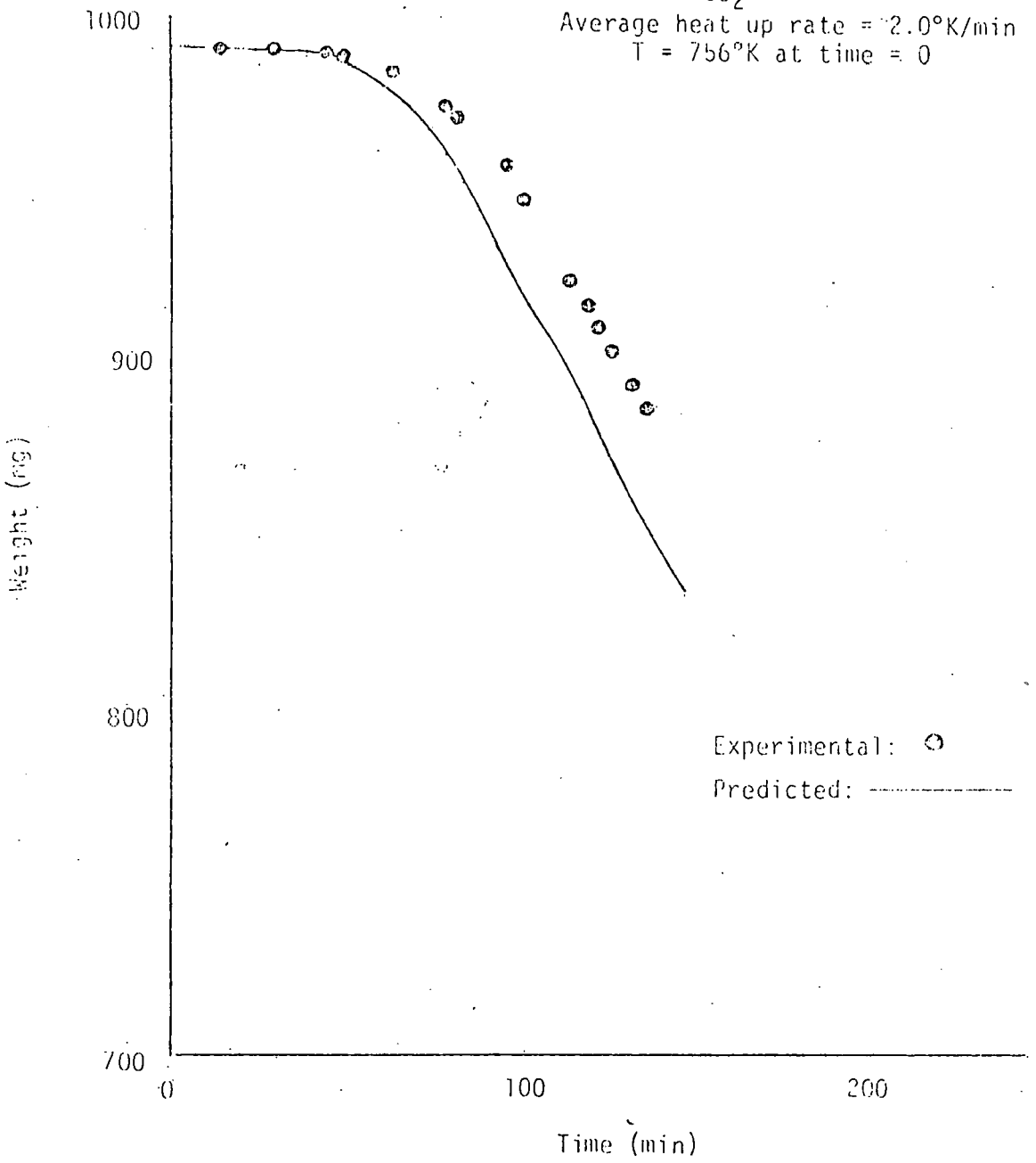

TABLE 9

Comparison of Model to Experimental Weight at the Point When Model Predicts Significant Silicate Formation*

Experiment	PCO_2 (atm)	Time (min)	Temp. (°K)	Experimental Weight (mg)	Predicted Weight (mg)
T-2	1.0	90	936	968	950
T-4	0.5	65	920	967	958
T-17	0.2	65	900	981	978
T-5	0.1	50	900	985	982

* More than 1 mg weight loss due to silicate formation.

As indicated in Table 9, high CO_2 partial pressures are inhibiting dolomite decomposition in some manner. What is missing and apparently needed is a separate determination of dolomite decomposition rates as a function of P_{CO_2}.

Mineral Decomposition in H_2O Environment. As mentioned earlier, the work conducted at LLL predicts significant enhancement of mineral decomposition rates in the presence of H_2O. Figure 25 shows the results of a non-isothermal experiment conducted in 0.5 atm H_2O. Since steam gasification would not occur to any appreciable extent until about t = 100 min, it appears as though the acceleration of mineral decomposition rates by steam is underestimated by LLL's rate expressions. Again, since it is primarily the low temperature predictions which are in error, the problem here too may be with an inadequate rate expressions for dolomite decomposition. In this case, it would seem that the presence of H_2O accelerates dolomite decomposition to a more significant degree than currently predicted.

Mineral Decomposition: H_2O - CO_2 Environment. Given the results above, it was decided to study mineral decomposition in an environment of .5 atm H_2O and CO_2. The results of a non-isothermal experiment are shown in Figure 26 and in this case the model predicts a significantly higher decomposition rate than is actually observed. Again, only dolomite decomposition is predicted to occur up to a time of about 80 minutes. Since earlier experiments indicated that the existing rate expressions *underestimated* the accelerating effect of steam, it appears as though the presence of CO_2 not only inhibits dolomite decomposition but it also prevents the acceleration effect of steam. It is not clear just how this mechanism operates and more research is needed

FIGURE 25

Sample Weight for Experiment T-7

P_{H_2O} = .5 atm

Average heat up rate = 2.1°K/min

T = 753°K at time = 0

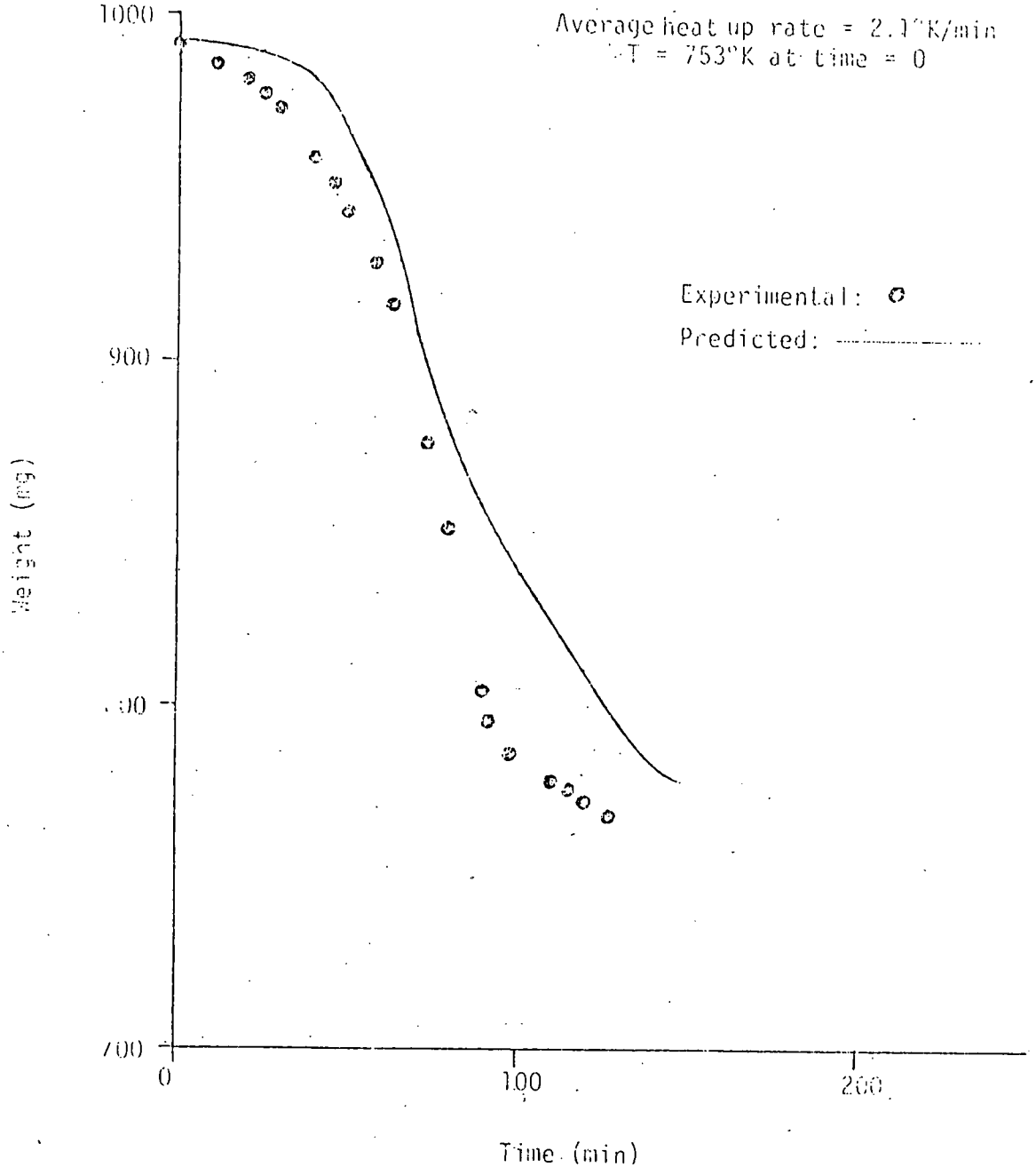

FIGURE 26

Sample Weight for Experiment T-3
P_{CO_2} = .5 atm, P_{H_2O} = .5 atm
Average heat up rate = 1.9°K/min
T = 761°K at time = 0

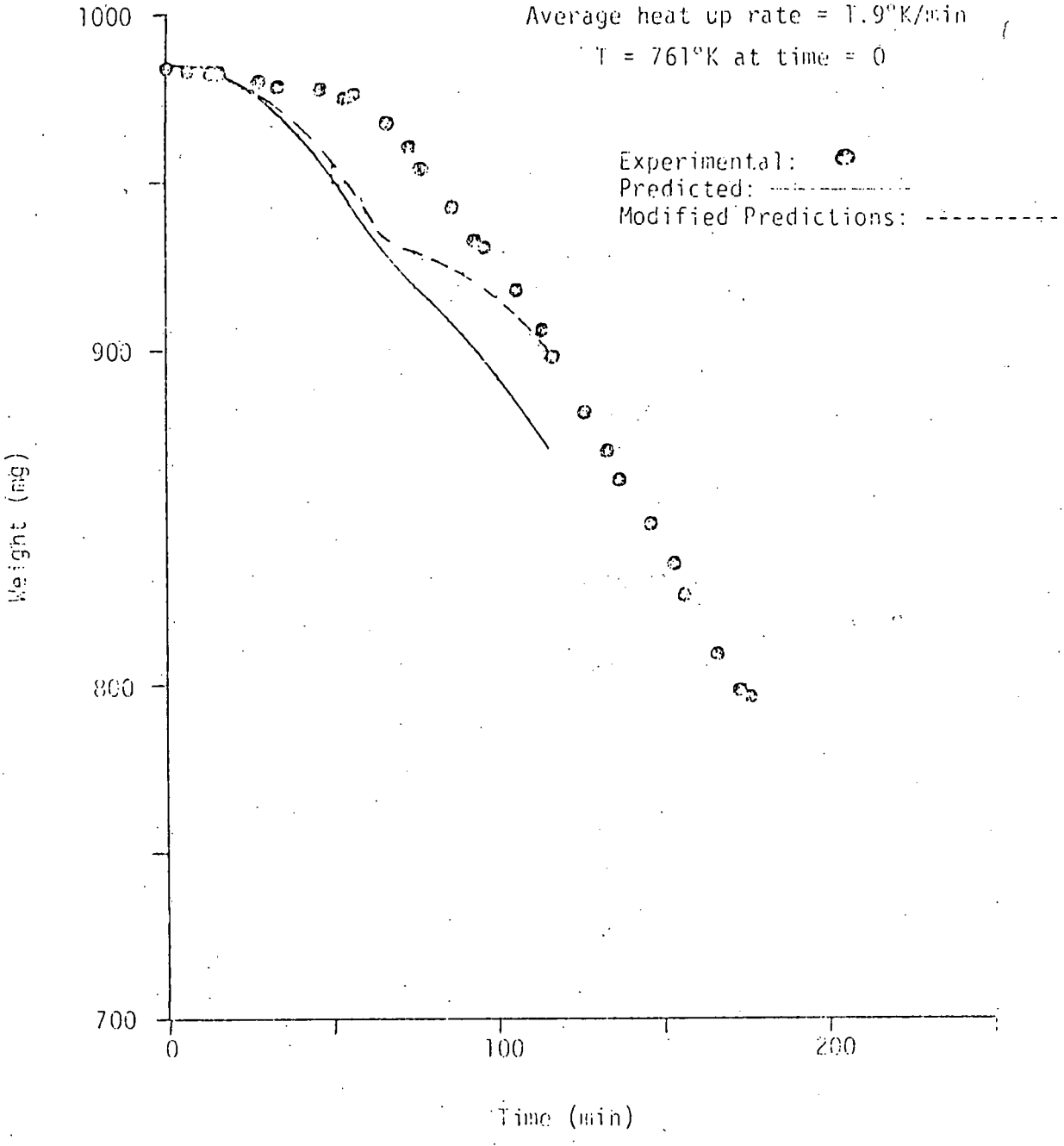

in order to develop a self consistent dolomite decomposition rate expression which can be safely extrapolated to other conditions.

The effect of CO_2 - H_2O mixtures on the rate of formation of silicates was also examined in a series of isothermal experiments conducted at 700 and 765 C. In every case there was excellent agreement between the predicted and measured rates and thus it is tentatively concluded that the existing rate expressions to predict silicate formation are adequate.

Char Gasification: H_2O - CO_2 Environment. The results of separate experiments to determine the kinetics of CO_2 - char and H_2O - char gasification have already been discussed. In both cases, the rates observed here were less than those predicted by LLL's rate expressions. In order to determine whether the two competing char reactions would behave the same during simultaneous reaction, a series of experiments were conducted using mixtures of CO_2 and H_2O in the inlet gas. Figure 27 shows a comparison of the measured and predicted char conversions for an experiment conducted at $P_{CO_2} = P_{H_2O} = 0.5$ atm. Also shown in this figure is the prediction assuming that only CO_2 gasification takes place. Note that an excellent match to the experimental data is obtained if the steam gasification rate is set equal to zero. Similar results are obtained during isothermal experiments as can be seen from Figure 28. Table 10 shows the average CO/H_2 ratio in the exit gas for a series of isothermal runs conducted in various CO_2 - H_2O concentrations.

TABLE 10

CO to H_2 Ratio for Isothermal Experiments
Containing Various Concentrations of CO_2 and Steam

Experiment Number	Feed Gas Composition	Temp. °K	Average CO/H_2 Ratio
T-8	50% CO_2/50% H_2O	980	0.56
T-9	8% CO_2/46% H_2O	980	0.28
T-10	50% CO_2/10% H_2O	980	4.40
T-14	50% CO_2/ 8% H_2O	1036	3.11
T-16	50% CO_2/ 50% H_2O	1042	0.40

FIGURE 27

Char Consumption for Experiment T-3

P_{CO_2} = .5 atm, P_{H_2O} = .5 atm

Average heat up rate = 1.9°K/min

T = 761°K at time = 0

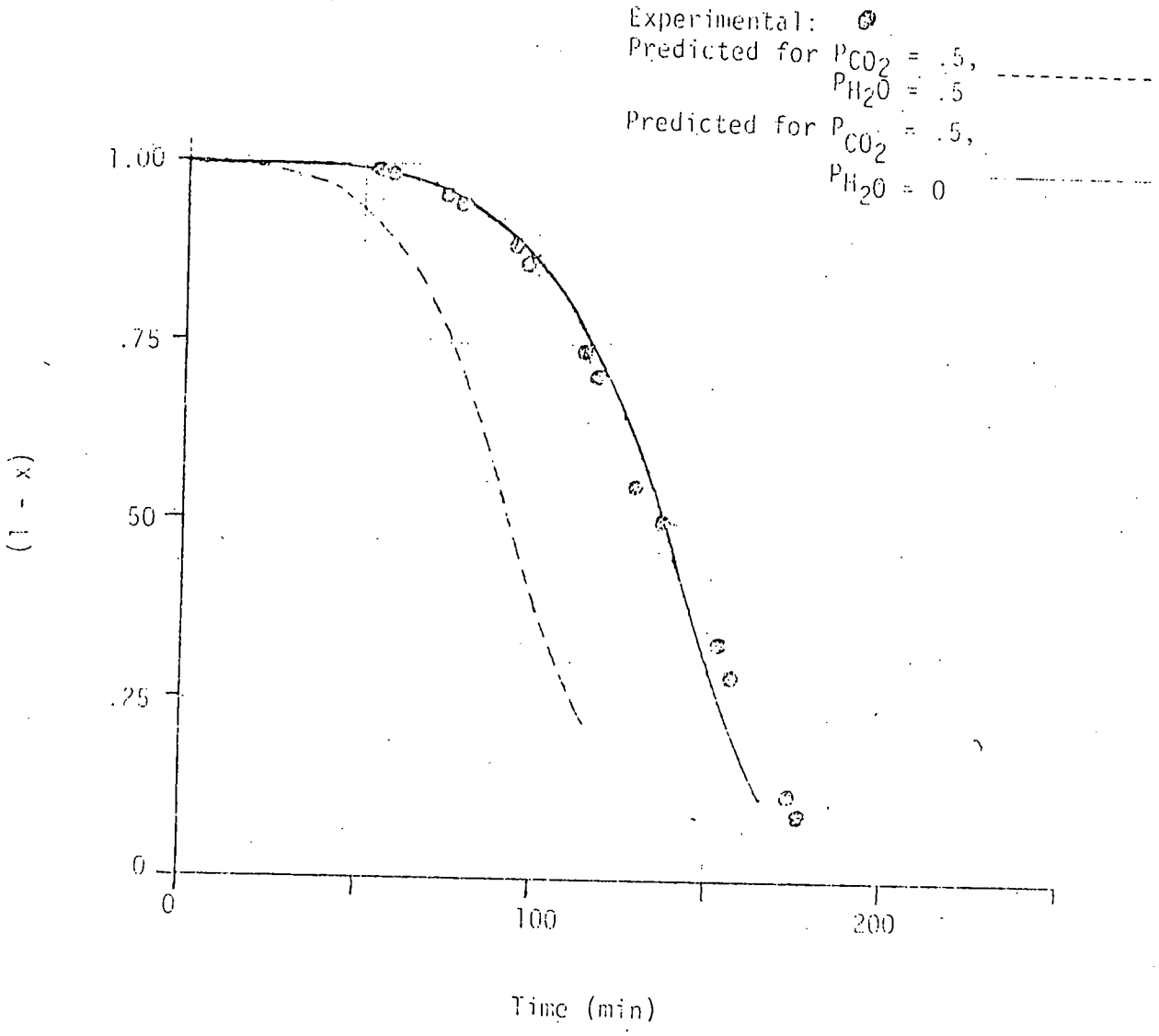

FIGURE 28

Char Consumption for Experiment T-8

P_{CO_2} = .5 atm, P_{H_2O} = .5 atm

T = 980°K

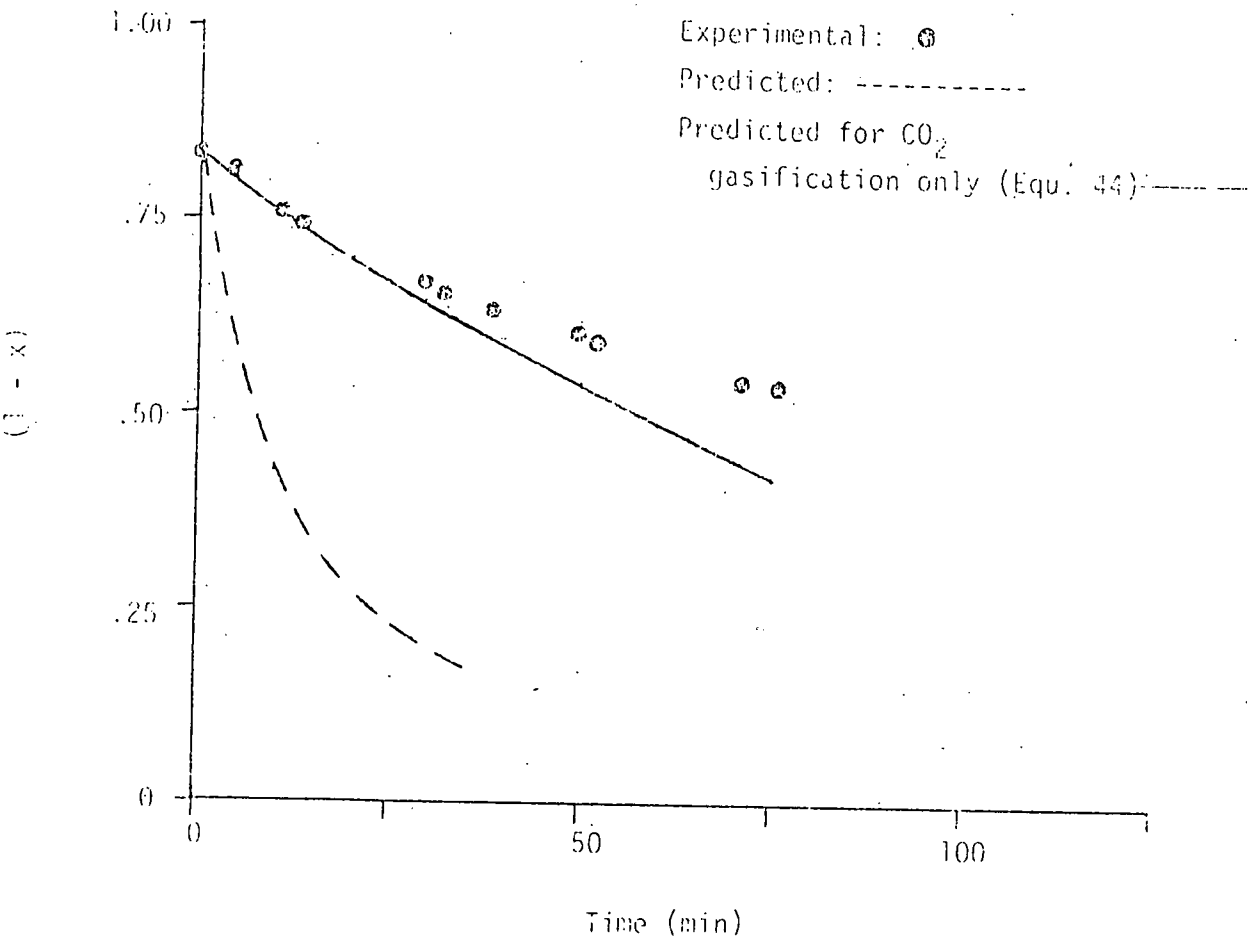

Note that there is still H_2 produced even though the model predicts a better match to the char conversion when it is assumed that no steam gasification takes place. This could be explained by the occurrence of the water gas shift reaction which would involve the reaction of the CO produced (by CO_2 gasification) with the H_2O present. Even still, the CO/H_2 ratios in Table 10 are a factor of 10-100 higher than is produced when there is an absence of CO_2 in the inlet gas. Obviously the CO_2 - char reaction is occurring to an appreciable extent.

Recall that all three reactions were used to derive the steam gasification rate expression in the work conducted here. On the other hand, LLL correlated their gasification data in a more empirical manner. Consequently one isothermal experiment was conducted at 760 C with P_{H_2O} = .37 atm. and P_{CO_2} = .09 atm and the resultant char conversion data were compared to the predictions of equations (51) and (57) - (59). Figure 29 shows this comparison, and as can be seen, the char consumption rate is matched more closely than it was when LLL's steam gasification rate expression was used. What is more, in this case the model predicts a *slower* rate than is measured. It is significant that in this case CO_2 gasification accounts for 20% of the char consumption whereas it was necessary to assume that it accounted for 100% when LLL's steam gasification expression was used.

Table 11 shows a comparison of the measured and predicted CO/H_2 ratios using the steam gasification kinetic expressions derived here.

TABLE 11

Measured and Predicted CO/H_2 Ratios (Avg.)

760 C, P_{H_2O} = 0.37 atm

P_{CO_2} (atm)	Experimental	Predicted
0	0.03	0.04
0.09	0.33	0.22

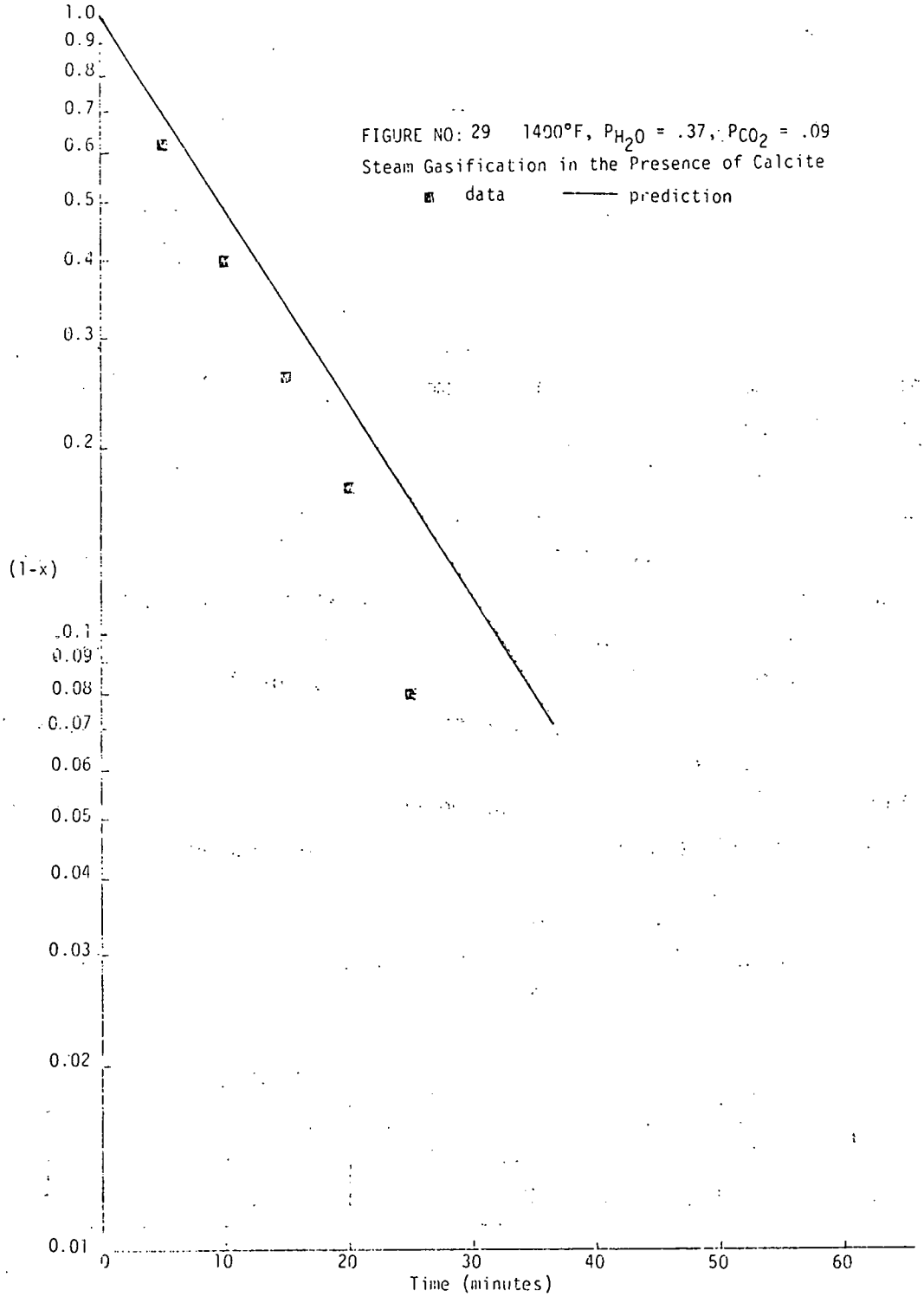

FIGURE NO: 29 1400°F, P_{H_2O} = .37, P_{CO_2} = .09
Steam Gasification in the Presence of Calcite
■ data —— prediction

As can be seen, reasonable matches to this ratio are also obtained. The differences between the measured and predicted ratios, as well as the discrepancies in the predicted char conversions are attributed to a lack of complete understanding of the water gas shift reaction rate and the role of the oxidation state of iron in catalyzing this reaction. In any case it appears that the steam gasification rates derived by LLL are inadequate in the presence of CO_2 - H_2O environments.

CONCLUSIONS

In view of the breadth of the material given in this report it is best to categorically list the conclusions which have been reached.

Retorting.....

The char produced when the shale was retorted at a slow rate (0.3°C/min) and in a low velocity purge stream (4 cm/min) was about 40% less active than char produced when *either* the retort or purge gas rates were higher.

Assay.....

There was no separate effect of shale assay (15-50 GPT) on the char oxidation kinetics. Assay was not examined with respect to char gasification or mineral decomposition reactions.

Char Oxidation.....

1. The following kinetic expression represents the intrinsic kinetics of shale as long as it is not thermally decarbonated

$$\frac{r_c}{C} = 8.47 \times 10^6 \exp\left[\frac{-23.2}{RT}\right] P_{O_2}$$

2. Strong evidence exists to indicate that CaO catalyzes char oxidation, perhaps by preferential chemisorption of oxygen.
3. The effective diffusivity of oxygen through the decharred mineral matrix was about three times lower for diffusion perpendicular to the bedding plane than for diffusion parallel to the bedding plane.
4. For large shale particles, gas-solid mass transport appears to contribute a major portion of the char oxidation resistance until about 40% of the char is consumed.

Mineral Decomposition.....

1. Recarbonation of calcite appears to be surface active and proceeds much faster if CO_2 is available on the surface (say, from char oxidation).
2. Separate calcite recarbonation kinetics experiments yielded a reversible rate expression which differs from that derived at Lawrence Livermore Laboratories (LLL).
3. There is evidence to suggest that the presence of CO_2 may

inhibit dolomite decomposition and also prevent steam from enhancing the decomposition rate.

4. Based on the limited experiments conducted here it appears that rate expressions derived at LLL underestimate the effect of steam on mineral decomposition rates but do a good job of predicting silication rates.

Char Gasification.....

1. An excellent match to CO_2 gasification rates was obtained with the following rate expression

$$\frac{r_c}{C} = \frac{4.68(10)^8 \exp[\frac{-44.3}{RT}] P_{CO_2}}{1 + 4.95 P_{CO_2}}$$

This expression predicts a rate which is a factor of three less than predicted by LLL.

2. The presence of CO was found to significantly inhibit CO_2 gasification although no attempt was made to quantify the degree of inhibition.

3. Steam gasification was found to involve three reactions in an involved series - parallel reaction sequence. The rate of the first reaction step ($C + H_2O \rightarrow CO + H_2$) could be described by

$$\frac{r_{sg}}{C} = 2100 \exp[\frac{-20.6}{RT}] P_{H_2O}^{.5}$$

4. The water gas shift reaction was found to proceed at fast rates, approaching equilibrium after about 20% of the char had been consumed. The CO/CO_2 ratios in the make-gas were typically on the order of 0.05. Iron, present in naturally occurring ankerite, was easily reduced by CO or H_2 and could be catalyzing the water gas shift reaction.

5. An empirical steam gasification rate expression derived at LLL predicts rates which are 3 to 10 times higher than those measured here. In addition, this rate expression predicts much faster char consumption rates in CO_2 - H_2O mixtures than were measured here. This is attributed to the empirical nature of the expression which does not account for the influence of the water gas shift reaction.

REFERENCES

1. Dockter, L., "Combustion of Oil Shale Carbon Residue", presented at the 68th Annual Meeting of the AIChE, Los Angeles, California, Nov. 20, (1975).
2. OIL & GAS JOURNAL, June 17, p. 26 (1974).
3. Burwell, E.L., and I.A. Jacobson, "Usable Gas From Oil Shale During Retorting", Bureau of Mines Tech. Progr. Report, TPR-85, Nov. (1974).
4. Burwell, E.L. and I.A. Jacobson, "Concurrent Gasification and Retorting of Oil Shale - A Dual Energy Source", presented at Rocky Mountain Regional Meeting of Soc. of Petr. Engrs. of AIME, paper no. SPE-5335, Denver, Colorado, April 7-9 (1975).
5. Berry, K.L., CHEM ENGR. PROG., 75, No. 9, p. 72, (1979).
6. Dougan, P.M., CHEM ENGR. PROG., 75, No. 9, p. 81, (1979).
7. Hubbard, A.B. and W.E. Robinson, "A Thermal Decomposition Study of Colorado Oil-Shale", Bureau of Mines Report of Investigation, RI-4744 (1950).
8. Allred, V.D., "Kinetics of Oil Shale Pyrolysis", CHEM. ENGR. PROG., 62, p. 55 (1966).
9. Arnold, C. "Effects of Heating Rate on the Pyrolysis of Oil Shale", presented at ACS meeting, Philadelphia, April 6-11, (1975).
10. Stout, N.D., Koskinas, G.H., Raley, J.H., Santor, S.D., Opela, R.J. and Rothman, A.J., Lawrence Livermore Laboratory, preprint, UCRL-77831, 27 April, 1976.
11. Burnham, A.K., Cedric T. Stubblefield and John C. Campbell, "Effects of Gas Environment on Mineral Reactions in Colorado Oil Shale," December 7, 1978, Preprint UCRL-81951 (Paper submitted to FUEL).
12. Juntgen, H. and K.H. Van Heek, "Non Isothermal Kinetics of Reversible Reactions Taking Place Taking as an Example the Thermal Decarbonation of $CaCO_3$" in Thermal Analysis, H. G. Weideman Ed. (Birkhauser, Verlag, Busel, 1972), p. 423.
13. Park, Won C., "Kinetics of Mineralogical Changes During Oil Shale Retorting", (1979) accepted for publication in "IN-SITU".
14. Jukkola, E.E., A.J. Denilanler, H.B. Jensen, W.I. Barnett, and W.I.R. Murphy, "Thermal Decomposition Rates of Carbonates in Oil Shale", Industrial and Engineering Chemistry, 45, 2711 (1953).
15. Campbell, J.H., "The Kinetics of Decomposition of Colorado Oil Shale: II Carbonate Minerals," March 13, 1979, UCRL-52089, Pt. 2.
16. Campbell, J.H. and A.K. Burnham, "Reaction Kinetics for Modeling Oil Shale Retorting", January 19, 1979, Preprint UCRL-81622 Rev. 1, (Paper submitted to IN-SITU).
17. Kridelbaugh, S.S., American Journal of Science, 273, 757 (1973).

18. Smoot, L.D. and D.T. Prath, Pulverized Coal Combustion and Gasification, Plenum Press (1979).

19. Ralston, O.C., Pike, R.D. and Duschak, L.H., Bureau of Mines Bulletin 236 (1925).

20. Young, D.A., Decomposition of Solids, (Pergammon Press, LTD., London, 1966).

21. Smith, J. Ward, W.A. Robb and N.B. Young, Laramie Energy Research Center, P.O. Box 3395, University Station, Laramie, WY 82701.

22. Mallon, R. G., Braun, R.L., Lawrence Livermore Laboratory, Preprint UCRL-77829, 1976.

23. Burnham, A.K. "Reaction Kinetics Between CO_2 and Oil Shale Residual Carbon. II, Partial Pressure and Catalytic Effects", January 18, 1979, Preprint UCRL-81335, pt. 2, (Paper submitted to FUEL).

24. Burnham, A.K., "Reaction Kinetics Between CO_2 and Oil Shale Residual Carbon. II, Partial Pressure and Catalytic Effects", July 11, 1978, Preprint UCRL-81335, pt. 2 (Paper submitted for FUEL).

25. "Operation of Coal Gasification Processes", Interim Report #1, R & D Report No. 66, part IV, p. 72, Office of Coal Research.

26. Schulmann, B.L., "Shale Matrix Plays an Important Role in Energy from Oil Shale", presented at 68th Annual AIChE Meeting, Los Angeles, Calif., Nov. 16-20, (1975).

27. Lewis, W.K., Gilliland, E.R. and H. Hipkin, IND & ENG. CHEM. 45, p. 1697 (1953).

28. Dent, F.J. and J.W. Cobb, J. AM. CHEM. SOC., p. 1903, (1929).

29. Weiss, C.V. and A.H. White, IND. & ENG. CHEM., 19, p. 882 (1927).

30. Fox, D.H. and A.H. White, IND & ENG. CHEM., 23, p. 259 (1931).

31. Fleer, A.W. and A.H. White, INC. & ENG. CHEM., 28, p. 1301 (1936).

32. Haynes, W.P., S.J. Glasior, and A.J. Forney, "Catalysis of Coal Gasification at Elevated Pressure", Bureau of Mines, Pittsburgh, Pa.

33. Taylor, H.S. and H.A. Neville, J. AM. CHEM. SOC., 43, p. 2055, (1921).

34. Wen, C.Y., O.C. Abraham and A.J. Talwalker, "Fuel Gasification," ADV IN CHEM SER. No. 69 , p. 251.

35. Johnson, J.L., "Coal Gasification," ADV IN CHEM SER. No. 131, p. 145.

36. Burnham, A.K. "Reaction Kinetics Between Steam and Oil Shale Char", Oct. 1978, preprint UCRL-81614 (Submitted to Chemical Society Meeting, Honolulu, Hawaii, April 1-6, 1979.)

37. Smith, J.M., "chemical Engineering Kinetics," 2nd Edition, McGraw-Hill, New York, 1970.

38. Slettvold, C.A., Biermann, A.H., Burnham, A.K., Lawrence Livermore Laboratory, Report UCRL-52619, 1978.

39. Schachter, Y., J. CATAL., 11, 147, 1968.

40. Levenspiel, O., "Chemical Reaction Engineering," John Wiley & Sons, New York, 1972.

41. Ranz, W.E., CHEM ENG. PROG., 48, p. 247, (1952).

42. Kunii, D. and Levenspiel, O., "Fluidization Engineering," Chap. 7, R.E. Kreiger Pub. Co., Huntington, New York, 1977.

43. Campbell, J.H., Lawrence Livermore Laboratory, to be published.

NOMENCLATURE

a	Activity
C	Char quantity
C_c	Char concentration
Co	Initial char quantity
D	Effective diffusivity of O_2, M^2/sec
E*	Activation energy, kcal/mole
F(t)	Dilution time function, eq. (37)
k	Rate constant, min^{-1}
k_g	Mass transfer coefficient, cm/sec
K	Adsorption constants, atm^{-1}
Keq	Calcite equilibrium constant, atm
Keqs	Water gas shift equilibrium constant
MCO_3	Moles $CaCO_3$ present
Pi	Partial pressure of "i", atm
R	Gas law constant, kcal/mole-°K
r_c	Char reaction rate, qty/min
r_s	Water gas shift reaction rate, moles/min
r_{sg}	Steam gasification reaction rate, qty/min
S	Active site
t	Reaction time, min
$\bar{t}$	Average residence time, min
T	Temperature, °K
X	Fraction char converted

☆ U.S. GOVERNMENT PRINTING OFFICE: 1980—640-258/2062